Applied Mathematical Modelling 36 (2012) 4760–4788

Contents lists available at SciVerse ScienceDirect

Applied Mathematical Modelling

journal homepage: www.elsevier.com/locate/apm

Design Element Concept of squeeze casting process

R. Ahmad [a,*], D.T. Gethin [b], R.W. Lewis [b]

[a] Department of Manufacturing and Industrial Engineering, Faculty of Mechanical and Manufacturing Engineering, Universiti Tun Hussein Onn Malaysia, 86400 Parit Raja, Batu Pahat, Johor, Malaysia

[b] Department of Mechanical Engineering, School of Engineering, Swansea University, Singleton Park, Swansea SA2 8PP, UK

ARTICLE INFO

Article history:
Received 15 November 2010
Received in revised form 15 November 2011
Accepted 1 December 2011
Available online 24 December 2011

Keywords:
Squeeze casting
Design sensitivity analysis
Design Element Concept

ABSTRACT

Design sensitivity analysis and the application of Design Element Concept have been explored. Exploration has focused on expressed sensitivity with respect to material property and shape of the coolant channel. The Design Element Concept has been applied to the die domain, since the design elements can be considered as a direct mapping of the blocks that make up a die. Analytical methods such as Direct Differentiation Method (DDM) and Adjoint Variable Method (AVM) have been employed in calculating the design element sensitivities. All the calculated design element sensitivities were verified with the Finite Difference Method and the results showed close agreement. From the design element sensitivities distribution in the die, the results show that convergence can be observed as more design elements are employed.

1. Introduction

The casting process is one of the oldest manufacturing processes. It is believed that the process was used by the Egyptians to make gold jewelry some 5000 years ago. Even though the process has a long history, its application is still relevant and it is being used today in many industries such as aerospace and automotive sectors to produce complex shape components. Direct squeeze casting is a combination of casting and forging processes. It is currently being employed to produce high performance and complex shape components such as steering, brake and suspension parts. It is also used for a family of rotational parts that have a complex cross section, but are essentially axisymmetric in form. These applications are due to the fact that the components produced from the squeeze forming process have several superior properties such as refined grain structure, improved mechanical strength and almost complete elimination of all shrinkage and gaseous porosity. These features are the outcome of the prolonged high contact pressure and intimate contact between the molten alloy and the metal die surfaces [1].

The major advantages claimed for the squeeze forming process over casting and forging can be listed as follows [2–4]:

(1) The ability to produce parts with complex profile and thin sections beyond the capability of conventional casting and forging techniques.
(2) Substantial improvement in material yield because of the elimination of gating and feeding systems.
(3) Significant reduction in pressure requirements, in comparison with conventional forging, while at the same time increasing the degree of complexity that can be obtained in the parts.

* Corresponding author. Tel.: +60 12 7196038; fax: +60 7 4536080.
E-mail address: rosle@uthm.edu.my (R. Ahmad).

0307-904X/$ - see front matter © 2011 Elsevier Inc. All rights reserved.
doi:10.1016/j.apm.2011.12.012

In the squeeze forming process, there are a number of process control parameters and these can be grouped under pressure cycle and cooling rate controls. For the latter, the die and coolant system design play a key role in achieving a defect free product. However, further complexity is introduced since these control groups interact. For example, it is evident from [5], that the pressure applied in the squeeze forming process has a direct effect on heat flux by influencing the heat transfer coefficient at the die–cast interface. This is due to the fact that any air gap evolution at the die–casting interface is controlled through pressure application. Similarly the position of cooling channels and the heat removal rates will have a significant impact on the temperature field within the die and hence the solidification of the squeeze formed part.

Design–simulate–evaluate–redesign is the standard procedure that is implemented in traditional optimisation that is carried out with the assistance of computational tools. It is executed until an acceptable design is achieved within the time scale that is available. This process is not only time consuming, it is also unlikely that a true optimum has been achieved. If this sequence can be fully automated, significant benefit will be derived. Numerical optimisation techniques were first explored in structural design in the early 80s [6]. During this period, a framework to undertake the process evolved and became established. It was, however, in the mid 90s when researchers started exploiting this framework in casting process simulation [7] and recently it is being explored for other applications, such as injection moulding and extrusion [8–10].

Optimisation studies have explored the application of a number of strategies. These include principally gradient methods and genetic algorithms. The former require the calculation of gradients that link design parameters with system response and combined with optimisation routines, they are used to find the best design according to a specified objective function and design variable constraints. Although they require gradient calculation, they are less computationally demanding, but are restricted in their search field. Genetic algorithms, also recognised as free-derivative methods, find the actual optimum based on a stochastic approach. They require more computational effort due to the use of a broader search field to find this solution.

The application of optimisation techniques to thermo-mechanical forming processes is particularly challenging due to the coupled and highly non-linear mechanisms that are present. However, optimisation of such processes is very desirable to facilitate high quality part manufacture and efficient process operation. For a prescribed part geometry, such optimisation will need to account for process setting changes as well as tooling design, i.e. shape. The current project will focus on the squeeze forming process.

As mentioned previously, optimisation depends on establishing design sensitivity expressed in terms of derivatives. In previous studies on process simulation, these have been estimated via difference equations and analytical equations have been developed in structural analysis. These have been shown to be advantageous and give accurate values of design sensitivity. Their application in process simulation has received little attention to date.

Some work in structural analysis has led to the concept of a design element. The design element represents a region of the structure and design sensitivity may be based on the design element, rather than the discretised element values that may be associated with the solution of the governing equations. Potentially this has advantages through reduction of computational effort in sensitivity calculation. It also offers the potential to undertake shape sensitivity analysis, for example a coolant channel may be treated as a design element and this may be positioned to achieve control over cooling behaviour. Again the application of this technique to simulation in highly nonlinear processes has received limited attention. Overall, little attention has been given to the use of a Design Element Concept that may prove to be attractive in reducing the effort that is required in computing sensitivity information.

To illustrate, structural optimisation was the first area in which the application of the optimisation technique was implemented. Typically, in a structural problem, the purpose of optimisation is to minimise for example, the weight of a structure or to maximise its stiffness. For example, Sienz and Hinton [11] described a reliable and robust tool for structural shape optimisation problem where the objective was minimisation of the volume of the connecting rod. This tool formed part of the integrated system ISO-P (2D) which stands for integrated structural optimisation package.

The combined influence of pressure and fill temperature also has a direct impact on the cooling rate within the squeeze cast part. In fact, cooling rate control plays a dominant role in achieving good mechanical property in the cast components. In connection with squeeze forming, Hwu et al. [12] discovered that high cooling rates improved the mechanical performance of the parts. In common with all rapid solidification technologies, it was found that the fast cooling rates reduced the grain size of the matrix which in turn raised the strength of the part. Kim et al. [13] found that the micro-structures of billets cast at pressures of 25, 50 and 75 MPa, respectively were more refined and dense than those of non-pressurised casts, because of a greater cooling rate. Maleki et al. [14] discovered that hardness of the samples (alloy LM13) steadily increases from 97 HB for the sample solidified under atmospheric pressure to about 110 HB at an external pressure of 171 MPa and becomes constant at higher applied pressures. Ideally, the cooling rate within the cast component should be identical throughout since this will be reflected in uniformity of mechanical properties.

Recently, a few works have explored the modelling of the complex physical phenomena associated with the squeeze forming process [15,16] to examine the contact behaviour between the die and cast part. These works primarily focused on a three dimensional thermo-mechanical analysis of the tool set and component. The starting point for this analysis was a full die, there was no consideration of fluid flow or displacement of the molten metal. In the former, Postek et al. [15] predicted the air gap in the squeeze forming processes from which the air gap had a direct influence on the interfacial heat transfer coefficient at the die–cast interface. It was found that squeeze formed parts solidify faster when compared with

the typical die cast part. This was concluded to be due to the small or close gap between the die and part which directly affected the interfacial heat transfer coefficient.

The coupling of optimisation techniques with process simulation is desirable and timely since computing power to undertake such analysis is becoming available and there is a growing industrial interest in this type of simulation. This is evident from the amount of research that has been carried out involving application of numerical optimisation in manufacturing processes such as extrusion, forging and metal forming processes.

A sensitivity analysis is central to any optimisation process. During the last decade, there have been many works on the application of design sensitivity analysis in connection with structural and manufacturing processes including metal forming processes. The latter present significant challenge due to the fact that metal forming processes require complex analysis since the nonlinearities that are present have to be taken into account. This includes for example friction, contact evolution at the tool-part interface and also material deformation behaviour. An example simulation development for a complex three dimensional part is presented in [17] that includes consideration of all key process parameters. These simulations required long processing times (several hours) to complete a single case study run. Such complexity and process time requirement is amplified when considering the calculation of sensitivity analysis itself which plays a vital role in gradient-based optimisation especially to ensure the accuracy of the sensitivity gradients. It is evident from the literature review that gradients may be derived in two basic ways, either, and most commonly as finite difference type expressions or as analytical expressions where the latter represent a reduced computing demand. These will be discussed within this section.

The analytical sensitivity analysis of a linear structural system has been explored in [18,19]. In [18], the parameter and shape sensitivities of linear structural analysis were covered in detail with a few numerical examples provided as benchmarks based on a cantilever truss, beam, plate and fillet. For the latter, procedures for structural analytical design sensitivity analysis of deformable solids with the finite element program POLSAP were described. The effectiveness of an Adjoint Variable Method (AVM) and a Direct Differentiation Method (DDM) depending on the number of design variables and constraints was discussed.

In connection with forming processes, Antunez and Kleiber [20] studied the sensitivity analysis of metal forming involving frictional contact under steady state conditions. The interest in such a model arose from the analysis of rolling processes and a two dimensional approach to cutting problems, where the contact zone was determined. They calculated sensitivities using the DDM. In comparison it was found that this gave a close result with the one performed using a Central Finite Difference Method (CFDM). The CFDM calculates the sensitivities numerically, where the equation is solved twice before and after perturbation. Thus, it suffers from two drawbacks, involving the accuracy of the calculated sensitivities due to the choice of the magnitude of perturbation and also it takes a longer time to calculate sensitivities because the finite element analysis has to be run twice at each iteration of the optimisation process. In contrast, DDM has absolute accuracy because of the analytical differentiation. Besides, the calculated sensitivities using DDM are faster than Finite Difference Method (FDM) because the sensitivities derived from DDM are obtained by solving the finite element equation only once at each iteration of the optimisation process. Antunez [21] has also extended his sensitivity analysis work to metal forming process that includes thermo-mechanical coupled analysis. Again, he used the DDM to perform the sensitivity gradients calculation. He considered the static yield stress and the heat transfer coefficient at the interface as the design variables and studied the sensitivity of temperature with respect to these design variables. In his work, all the results obtained by DDM were checked and compared with the FDM in which he found that the results showed close agreement.

Kim and Huh [22] applied design sensitivity analysis to the sheet metal forming processes. A design sensitivity analysis scheme was proposed for an elasto-plastic finite element analysis with explicit time integration using the DDM to perform the sensitivity calculation. The DDM was used to deal with the large deformation. The result obtained using the DDM was compared with the result obtained from FDM in the drawing of a cylindrical cup and a 'U-shaped' bend. The results showed close agreement, thus demonstrating the accuracy of the calculated analytical DDM.

Smith et al. demonstrated the application of sensitivity analysis to the optimal design of polymer extrusion [23,24]. For the former, the work focused on sensitivity analysis for nonlinear steady-state systems. In this work, the sensitivities were derived using both the DDM and the AVM. In this work it was found that the two sensitivity analysis methods yielded identical expressions. The design variables were die thickness and prescribed inlet pressure. These were optimised to minimise pressure drop and to generate an uniform velocity across the die exit. It was summarised that sensitivities derived from the FDM for this nonlinear problem were both inaccurate and inefficient.

The design element is a concept where the sensitivities are calculated based on predefined zones, possibly identified by a die designer. These sensitivities are used by supplying them to the optimisation routines to achieve the optimal solution. It is potentially useful in a way that since a die is constructed from a number of steel blocks, this allows some pre-selection of the zones of steel blocks based on the zones defined for the design elements in a die. The Design Element Concept was clearly defined in 1989 where the key nodes of the design elements can be treated as design variables for shape optimisation problems. Arora [25] defined two levels of discretisation, the first level corresponded to the finite element model for analysis, and the second level corresponded to the design element model for optimisation. He applied the Design Element Concept to the fillet shape design problem, where his objective was to minimise the volume of the piece and he successfully achieved a reduction of 8.5% from the initial volume. However, little attention has been given to the use of the Design Element Concept in optimisation. The Design Element was first applied to the optimisation of plate and shell structures [26]. Botkin [26] used this scheme to define the domain of a plate with two holes under tensile load. In his work, he introduced the concept of a plate or shell shape design element. He used the Design Elements to change the plate shape by adjusting the boundaries of

the element. This work featured the use of four design elements to capture the fillet plate, there have been fewer studies that use a number of design elements to map a part geometry.

Based on the previous works, no attention has been given to the parameter Design Element Concept, especially on the decision of how the design elements may be mapped on to the domain under consideration. Further, the shape Design Element Concept has not been applied in squeeze casting process simulations and thus this new application will be discussed in the subsequent sections.

2. Research methodology

Simulation of all forming processes is particularly demanding since they are inherently complex and non linear. The cooling and solidification cycle in the casting process can be described by the transient energy equation which in the absence of convection may be written [27],

$$\nabla \cdot [k(T)\nabla \dot{T}] + Q = \rho c(T)\dot{T}, \tag{1}$$

where k is the conductivity, T is the unknown temperature field, Q is the heat generation, ρ is the density, c is the specific heat and $\dot{T}$ is the derivative of temperature with respect to time.

In Eq. (1), the conductivity and heat capacity are temperature dependent.

Boundary conditions are required in time and space, thus initial, Dirichlet and Neumann boundary conditions for this system are described as follows [28] within a cylindrical framework. This has been chosen to address the axisymmetric part family where further simplification follows from elimination of any angular variations. The technique can be extended in principle to other coordinate frameworks.

Initial boundary condition

$$T(r,\theta,z,0) = T_0(r,\theta,z) \quad \text{in } \Omega$$

where r, θ and z are the coordinates axis, T_0 is the prescribed temperature distribution in Ω and Ω is the domain.

Dirichlet boundary Condition

$$T = T(r,\theta,z,t) \quad \text{on } \Gamma_T$$

where r, θ and z are the coordinates axis, t is the time and Γ_T is the boundary curve where the essential boundary condition is applied.

Neumann boundary condition

$$q = -k\frac{\partial T}{\partial n} \quad \text{on } \Gamma_q,$$

where q is the heat outflow in the direction n normal to the boundary Γ_q, k is the conductivity, $\frac{\partial T}{\partial n}$ is the partial derivative of temperature in normal direction and Γ_q is the boundary curve where the natural boundary condition is applied.

In the case of phase transformation, the enthalpy method was applied [27]. The essence of the application of the enthalpy method is the involvement of a new variable, enthalpy, denoted by H, such that, $\rho c = dH/dT$, Eq. (1) is transformed to the following form

$$\nabla \cdot [k(T)\nabla T] + Q = \frac{\partial H}{\partial T}\dot{T}. \tag{2}$$

The definition of the enthalpy for a metal alloy is given as follows [26]:

$$H(T) = \int_{T_r}^{T_s} \rho c_s(T)dT + \rho L + \int_{T_s}^{T_l} \rho c_f(T)dT + \int_{T_l}^{T} \rho c_l(T)dT \quad (T \geqslant T_l), \tag{3}$$

$$H(T) = \int_{T_r}^{T} \rho c_s(T)dT + \int_{T_s}^{T} \left(\rho\left(\frac{dL}{dT}\right) + \rho c_f(T)\right)dT \quad (T_s \leqslant T \geqslant T_l), \tag{4}$$

$$H(T) = \int_{T_r}^{T} \rho c_s(T)dT \quad (T \leqslant T_s), \tag{5}$$

where subscripts l and s refer to liquid and solid respectively, ρ is the density (constant), L is the latent heat. C_f is the specific heat in the freezing region and T_r is a reference temperature lower that T_s, generally 25 °C.

Enthalpy may be computed in a number of ways, however, due to its improved accuracy in tracking the phase change inside the metal alloy, the following averaging formula [27] was used for the estimation of the enthalpy variable

$$\rho c \simeq \left(\frac{\left(\frac{\partial H}{\partial x}\right)^2 + \left(\frac{\partial H}{\partial y}\right)^2}{\left(\frac{\partial T}{\partial x}\right)^2 + \left(\frac{\partial T}{\partial y}\right)^2} \right)^{\frac{1}{2}}. \tag{6}$$

By employing the weighted residual method and the standard Galerkin technique [28], Eq. (2) is transformed to yield the following linear system of equations [27],

$$\boldsymbol{C}(\boldsymbol{T})\{\dot{\boldsymbol{T}}\} + \boldsymbol{K}(\boldsymbol{T})\{\boldsymbol{T}\} = \boldsymbol{F}, \tag{7}$$

where $\boldsymbol{K}$ and $\boldsymbol{C}$ are the conductivity and heat capacity matrices. $\boldsymbol{F}$ is the thermal loading vector. For an axi-symmetric framework, $\boldsymbol{C}$, $\boldsymbol{K}$ and $\boldsymbol{F}$ are defined as follows:

$$\boldsymbol{C}(T) = \sum_e \int_{\Omega_e} \rho c N_i^e N_j^e \, d\Omega \tag{8}$$

$$\boldsymbol{K}(T) = \sum_e \int_{\Omega_e} \left[k \frac{\partial N_i}{\partial r} \frac{\partial N_j}{\partial r} + k \frac{\partial N_i}{\partial z} \frac{\partial N_j}{\partial z} \right] d\Omega + \sum_e \int_{\Gamma_{he}} N_i h_c N_j \, d\Gamma, \tag{9}$$

$$\boldsymbol{F} = \sum_e \int_{\Gamma_{he}} N_i^e h_c T_\infty \, d\Gamma - \sum_e \int_{\Gamma_{qe}} N_i^e q \, d\Gamma, \tag{10}$$

$$d\Omega = 2\pi r \, dr \, dz, \tag{11}$$

$$d\Gamma = 2\pi r (dr^2 + dz^2)^{1/2}. \tag{12}$$

For the conductivity matrix, the first term is due to the diffusive part whereas the second is due to convection, either to the surroundings or to the coolant channels.

A finite difference approximation was used for the temporal discretisation [27]

$$\left[\frac{C_{n+\alpha}}{\Delta t} + \alpha K_{n+\alpha} \right] (T_{n+1}) = \left[\frac{C_{n+\alpha}}{\Delta t} - (1-\alpha) K_{n+\alpha} \right] (T_n) + (F_{n+\alpha}) \tag{13}$$

and a Crank Nicolson scheme [27] where $\alpha = 0.5$ was used for the time marching scheme. The Crank Nicolson scheme was chosen due to its balance between accuracy and stability as opposed to other schemes such as Forward Euler and Backward Euler schemes.

2.1. Interfacial heat transfer between two parts in contact

Modelling of the heat transfer phenomenon between the die and casting plays an important role in obtaining accurate simulation of the cooling behaviour in a casting component. This is particularly relevant for the squeeze forming process in which control of thermal response through application of a pressure cycle is critical to process success. Heat transfer can also take place between the blocks that make up the die itself. Interfacial heat transfer may be handled in a number of ways within a numerical scheme, for example in a finite element formulation thin elements may be introduced at this interface, where they act as a layer between casting and die. It is also possible to use a coincident node approach that represents an interfacial element of zero thickness. In this work, the heat transfer at the die–casting interface is modelled using a convection heat transfer type mechanism [29]. This has been done to deal with the situation where nodes in the die and casting are not constrained to be coincident, hence simplifying the finite element meshing and remeshing requirements making it suited to the design element approach.

One of the attractive features in implementing this model is that there is no need to introduce additional elements. The interface surfaces interact naturally with each other. In two dimensions, any two parts in contact with each other, for example a casting and its die, are separated by an interface boundary line. This is illustrated in Fig. 1.

The interface boundary can be divided into a number of segments and these segments can capture different interface conditions. Common to all segments is that one part of the interface represents the casting surface and the other is the die. During analysis, strategically each boundary segment in the die, the corresponding boundary segment in the casting acts as a reference condition and vice versa. In detail, at the interface boundary, the reference temperature in the die is obtained by taking the averaged closest two nodal temperatures at the casting interface. This approximates the die reference temperature at the interface. The same implementation is applied for the reference temperature in the casting by considering the averaged closest two nodal temperatures at the die interface.

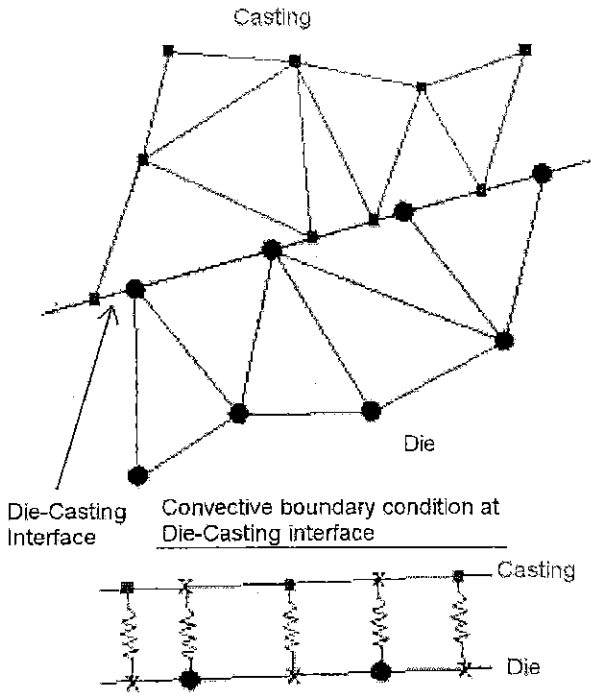

Fig. 1. Schematic of interface model.

2.2. Sensitivity analysis

Gradient-based optimisation is one of the most popular strategies in tackling optimisation in engineering design problems. The calculation of sensitivity gradients is a core requirement for optimisation. Such calculations can be computationally demanding and any strategy that will reduce this demand is attractive. This has led to exploration of a Design Element Concept. The application of the Design Element Concept including the parameter and shape sensitivities will be discussed in the following sections.

In standard design sensitivity analysis, sensitivity gradients are calculated for each discretised element in the domain. However, the Design Element Concept allows the design sensitivity gradients to be calculated based on zones of design elements, thus reducing the design sensitivity loop calculation that significantly decreases the demands for the optimisation process.

2.3. Analytical methods

Where they may be applied, analytical methods have an advantage over Finite Difference Methods (FDM) due to their accuracy and efficiency in performing the gradient calculations. This is further amplified for nonlinear problems where the FE analyses are expensive. The optimisation of nonlinear problems has been explored in metal forming processes, polymer extrusion and casting processes. There are two types of analytical methods; namely the Direct Differentiation Method (DDM) and the Adjoint Variable Method (AVM). Generally, the DDM is used if the number of Design Constraints (DC) is greater than the Number of Design Variables (NDV). In the DDM, the derivatives of the response with respect to design variables are solved as many times as there are design variables. Thus, the DDM is used if NDV < DC. In the AVM, the adjoint equation is solved as many times as there are design constraints. Therefore, it is efficient to find the design sensitivity gradients using the AVM if DC $\leqslant$ NDV.

2.3.1. Direct Differentiation Method (DDM)

The DDM can be illustrated through consideration of the general matrix equation that includes a vector containing design variables,

$$\boldsymbol{K}(\boldsymbol{b})\boldsymbol{q} = \boldsymbol{F}, \tag{14}$$

where $\boldsymbol{b}$ is the design variable vector, $\boldsymbol{q}$ is the displacement vector, $\boldsymbol{F}$ is the global force vector and $\boldsymbol{K}$ is the global stiffness matrix. The goal is to find the sensitivity of a function $\psi(\boldsymbol{q}(\boldsymbol{b}), q_a, \sigma(b), \sigma_a, \boldsymbol{b})$ with respect to the design variables $\boldsymbol{b}$,

$$\nabla_b \psi \text{ subject to } \boldsymbol{K}(\boldsymbol{b})\boldsymbol{q} = \boldsymbol{F}, \tag{15}$$

where $\nabla_b\psi$ is defined as

$$\nabla_b\psi = \left[\frac{\partial\psi}{\partial \boldsymbol{b}_1}\ \frac{\partial\psi}{\partial \boldsymbol{b}_2}\cdots\frac{\partial\psi}{\partial \boldsymbol{b}_n}\right]. \tag{16}$$

q_a is the displacement constraint and σ_a is the von Mises stress constraint. Assuming that the $\boldsymbol{K}$ matrix is not singular, both sides of the equilibrium equation are differentiated with respect to $\boldsymbol{b}$. The following expression for $\nabla_b q$ can be derived:

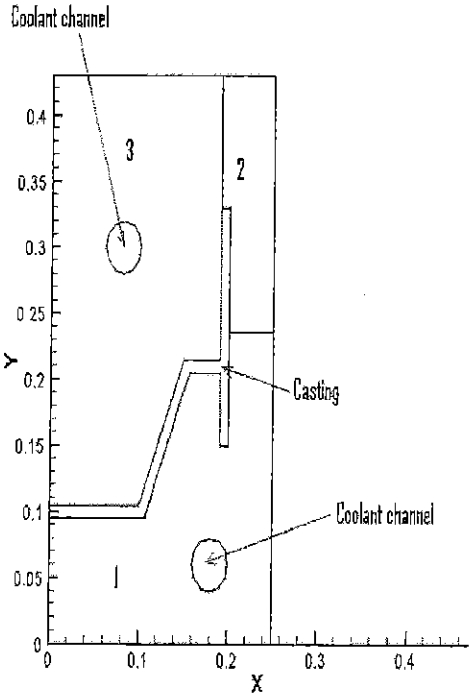

Fig. 2. The division of zones in the die for 3 design elements.

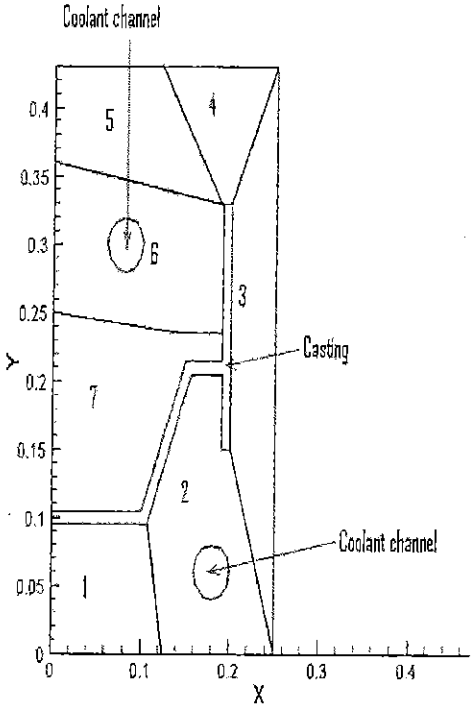

Fig. 3. The division of zones in the die for 7 design elements.

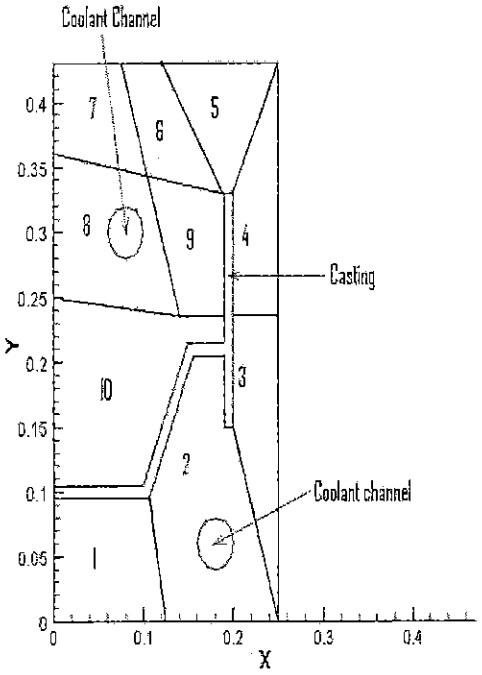

Fig. 4. The division of zones in the die for 10 design elements.

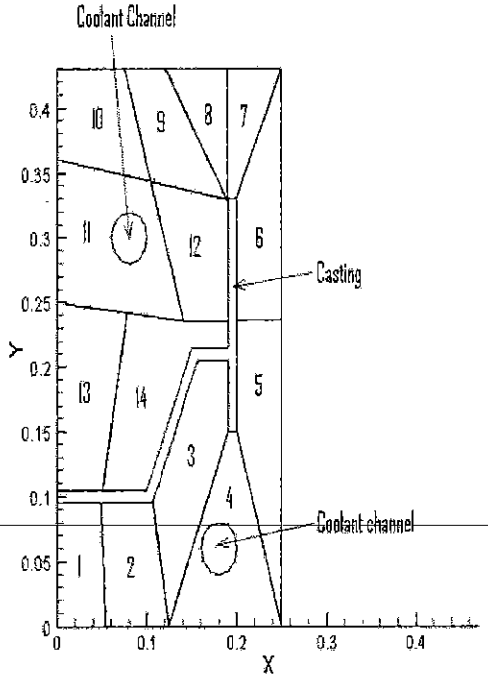

Fig. 5. The division of zones in the die for 14 design elements.

$$\nabla_b \boldsymbol{q} = \boldsymbol{K}^{-1}\left[\nabla_b \boldsymbol{F} - \nabla_b\left(\sum \boldsymbol{K}_{de}\boldsymbol{q}\right)\right], \tag{17}$$

where $\boldsymbol{K}_{de}$ represents the discretised elements in the defined design elements. In the following examples, the die has been divided into zones of 3, 7, 10, 14 and 28 design elements. This has been chosen to see the difference in the calculated sensitivities for different sub-divisions of design elements in the die. Figs. 2–6 show the divisions of the zones in the die for 3, 7, 10, 14 and 28 design elements. The design elements are clearly chosen to provide a thermal interface between the die and part as control of this is required to ensure success of the process. The method for handling this interface has been set out

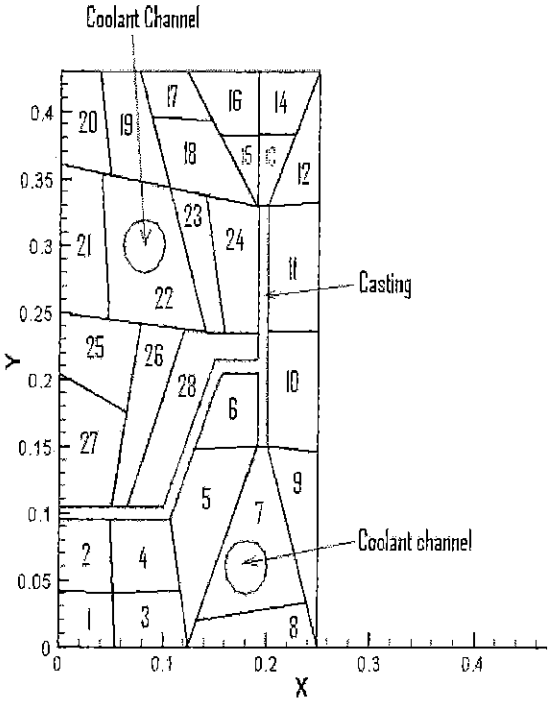

Fig. 6. The division of zones in the die for 28 design elements.

earlier in the paper. Generally the design elements do not capture the thermal interface between blocks, however the approach is capable of handling this through extension of the principles applied at the die to casting interface. Treatment of structural contact between the die blocks has been excluded from this model. This simplification was chosen because the aim of the study was to explore the Design Element Concept rather than address the full complexity of the process, possibly within a three dimensional framework. This could be a follow on project by incorporation into the scheme described in [17].

The design element sensitivity gradient for each design element is merely the summation of the derivatives of the stiffness matrices $\sum \boldsymbol{K}_{de}$ for the discretised elements inside the particular design element. This follows the finite element method procedure where the total stiffness matrix of the structure is the summation of the individual finite element stiffness matrix in the domain.

The exact sensitivities of $\psi\ (\boldsymbol{q}(\boldsymbol{b}), q_a, \sigma(b), \sigma_a, \boldsymbol{b})$ can be calculated by substituting $\nabla_b \boldsymbol{q}$

$$\nabla_b \psi = \nabla_b^e \psi + \nabla_q \psi \cdot \nabla_b \boldsymbol{q}, \tag{18}$$

where $\nabla_b^e \psi$ is the gradient term for the explicit dependence of $\psi\ (\boldsymbol{q}(\boldsymbol{b}), q_a, \sigma(b), \sigma_a, \boldsymbol{b})$ on $\boldsymbol{b}$.

For a von Mises stress constraint, the exact sensitivities of $\psi\ (\boldsymbol{q}(\boldsymbol{b}), q_a, \sigma(b), \sigma_a, \boldsymbol{b})$ can be calculated by substituting $\nabla_b \boldsymbol{q}$

$$\nabla_b \psi = \nabla_b^e \psi + \nabla_\sigma \psi \cdot \nabla_q \boldsymbol{\sigma} \cdot \nabla_b \boldsymbol{q}. \tag{19}$$

2.3.2. Adjoint Variable Method (AVM)

For the AVM, firstly, an augmented functional is defined,

$$L(\boldsymbol{q}, \boldsymbol{b}, \lambda) = \psi - \lambda^T (\boldsymbol{K}\boldsymbol{q} - \boldsymbol{F}), \tag{20}$$

where λ is a Lagrange multiplier vector and the additional condition is the equilibrium equation.

From the stationary condition,

$$\frac{\partial L}{\partial \boldsymbol{q}} = 0. \tag{21}$$

Differentiating the augmented functional with respect to the design variable gives

$$\frac{dL}{d\boldsymbol{b}} = \frac{d\psi}{d\boldsymbol{b}} - \lambda^T \frac{d}{d\boldsymbol{b}} (\boldsymbol{K}\boldsymbol{q} - \boldsymbol{F}). \tag{22}$$

Since the state equation holds,

$$\frac{dL}{d\boldsymbol{b}} = \frac{d\psi}{d\boldsymbol{b}}. \tag{23}$$

Defining the sensitivity of the augmented functional with respect to the design variable vector leads to

$$\frac{dL}{d\boldsymbol{b}} = \frac{\partial L}{\partial \boldsymbol{b}} + \frac{\partial L}{\partial \boldsymbol{q}} \frac{d\boldsymbol{q}}{d\boldsymbol{b}}. \tag{24}$$

By exploiting the stationary condition, the adjoint vector can be written as follows:

$$\boldsymbol{K}\lambda = \frac{\partial \psi}{\partial \boldsymbol{q}}. \tag{25}$$

For the von Mises stress constraint, again, by exploiting the stationary condition, the adjoint vector can be written as follows:

$$\boldsymbol{K}\lambda = \frac{\partial \psi}{\partial \sigma} \cdot \frac{\partial \sigma}{\partial \boldsymbol{q}}. \tag{26}$$

So, to obtain the sensitivities it is enough to find the partial design derivatives of the augmented functional, then

$$\frac{d\psi}{d\boldsymbol{b}} = \frac{\partial \psi}{\partial \boldsymbol{b}} + \lambda^T \left(\frac{\partial \boldsymbol{F}}{\partial \boldsymbol{b}} - \frac{\partial \boldsymbol{K}}{\partial \boldsymbol{b}} q \right). \tag{27}$$

The sensitivity for each design element is merely the summation of the individual discretised element sensitivity inside that particular design element. Again, this reflects the assembly of the global stiffness matrix as used in the finite element method.

2.4. Finite Difference Method (FDM)

The FDM is the simplest way to calculate sensitivity values due to the fact that, unlike the DDM and AVM, it does not require a direct access to the finite element source code. However it suffers from a few drawbacks as discussed in previous section, notably involving the accuracy of the calculated sensitivities and also it takes longer time to calculate sensitivities due to the fact that the finite element equation has to be solved twice at each iteration of the optimisation process. However, in order to benchmark the calculated sensitivities using the analytical methods, it is necessary to derive the sensitivities using the FDM.

In this work, to facilitate comparison, the design sensitivities for displacements and stresses are computed using two techniques, which are forward FDM and central FDM. For the forward FDM [30], the approximation of design sensitivities for displacement is given as

$$\frac{\partial \boldsymbol{q}^i}{\partial \boldsymbol{b}_j} \approx \frac{\boldsymbol{q}^i(\boldsymbol{b} + \Delta \boldsymbol{b}) - \boldsymbol{q}^i(\boldsymbol{b})}{\Delta \boldsymbol{b}}, \tag{28}$$

where $\boldsymbol{q}^i(\boldsymbol{b} + \Delta \boldsymbol{b})$ is obtained by solving the following equation,

$$\boldsymbol{K}(\boldsymbol{b} + \Delta \boldsymbol{b})\boldsymbol{q}(\boldsymbol{b} + \Delta \boldsymbol{b}) = \boldsymbol{F}(\boldsymbol{b} + \Delta \boldsymbol{b}). \tag{29}$$

For stress sensitivities, the approximation is given as

$$\frac{\partial \sigma^i}{\partial \boldsymbol{b}_j} \approx \frac{\sigma^i(\boldsymbol{b} + \Delta \boldsymbol{b}) - \sigma^i(\boldsymbol{b})}{\Delta \boldsymbol{b}} \tag{30}$$

and $\sigma(\boldsymbol{b} + \Delta \boldsymbol{b})$ is obtained from,

$$\sigma(\boldsymbol{b} + \Delta \boldsymbol{b}) = \boldsymbol{D}(\boldsymbol{b} + \Delta \boldsymbol{b})\boldsymbol{B}(\boldsymbol{b} + \Delta \boldsymbol{b})\boldsymbol{q}(\boldsymbol{b} + \Delta \boldsymbol{b}). \tag{31}$$

For the central FDM, the design sensitivities of displacements and stresses are approximated as

$$\frac{\partial \boldsymbol{q}^i}{\partial \boldsymbol{b}_j} \approx \frac{\boldsymbol{q}^i(\boldsymbol{b} + \Delta \boldsymbol{b}) - \boldsymbol{q}^i(\boldsymbol{b} - \Delta \boldsymbol{b})}{2\Delta \boldsymbol{b}}, \tag{32}$$

$$\frac{\partial \sigma^i}{\partial \boldsymbol{b}_j} \approx \frac{\sigma^i(\boldsymbol{b} + \Delta \boldsymbol{b}) - \sigma^i(\boldsymbol{b} - \Delta \boldsymbol{b})}{2\Delta \boldsymbol{b}}, \tag{33}$$

where $\boldsymbol{q}(\boldsymbol{b} - \Delta \boldsymbol{b})$ and $\sigma(\boldsymbol{b} - \Delta \boldsymbol{b})$ are obtained from,

$$\boldsymbol{K}(\boldsymbol{b} - \Delta \boldsymbol{b})\boldsymbol{q}(\boldsymbol{b} - \Delta \boldsymbol{b}) = \boldsymbol{F}(\boldsymbol{b} - \Delta \boldsymbol{b}), \tag{34}$$

$$\sigma(\boldsymbol{b} - \Delta \boldsymbol{b}) = \boldsymbol{D}(\boldsymbol{b} - \Delta \boldsymbol{b})\boldsymbol{B}(\boldsymbol{b} - \Delta \boldsymbol{b})\boldsymbol{q}(\boldsymbol{b} - \Delta \boldsymbol{b}). \tag{35}$$

2.5. Parameter design sensitivity analysis

In parameter design sensitivity analysis, there are a number of design variables that may be considered as discussed earlier in previous section. In this work, Young modulus was considered as the parameter design variable, chosen because it has a significant effect on the results as compared to other design variables. This is due to the direct dependency of the stress

field on the associated strain and modulus values. Exploring the impact of Young modulus is rather hypothetical, because dies are usually fabricated from steel which dictates thermomechanical parameters within practical limits. However the choice of materials, such as alloys that have thermal properties that facilitate rapid heat removal at strategic locations within the die may be of interest (implying strong modulus gradients). Young modulus will be used in this work as a means of investigating the simulation approach. This is also quite relevant in the design sensitivity analysis using the Design Element Concept, since a die is typically fabricated based on a number of blocks (with the potential for using different materials) and it is particularly useful in a way that the defined zones using the Design Element Concept can be considered as a direct mapping to a number of blocks that make up the die.

2.5.1. The stiffness matrix derivative for parameter sensitivity

The key factor in the calculation of sensitivities using the analytical methods is to formulate the derivative of the stiffness matrix with respect to the design variable. For example, considering the Young modulus, E, the stiffness matrix derivative is given by

$$\frac{\partial \mathbf{K}}{\partial E} = \mathbf{B}^T \frac{\partial D}{\partial E} \mathbf{B} \mathbf{J}_D \pi \mathbf{r}_{bar}. \tag{36}$$

From the equation above, it can be seen that only the D matrix is differentiated with respect to the Young modulus because it only appears in this matrix.

2.5.2. The derivative of von Mises stress with respect to displacement vector

It can be seen from the derivations of the DDM and the AVM that the derivative of von Mises stress with respect to displacement vector is present in both methods. Thus, this section focuses on this derivation. For an axi-symmetric problem, the von Mises stress is given by [31,32]:

$$\sigma_e = \sqrt{\sigma_r^2 + \sigma_\theta^2 + \sigma_z^2 + 3\tau_{rz}^2 - \sigma_r\sigma_\theta - \sigma_r\sigma_z - \sigma_\theta\sigma_z}. \tag{37}$$

By using the chain rule of differentiation, the derivative of the von Mises stress with respect to the displacement vector is given as:

$$\frac{\partial \sigma_e}{\partial \mathbf{q}} = \frac{\partial \sigma_e}{\partial \sigma_r}\frac{\partial \sigma_r}{\partial \mathbf{q}} + \frac{\partial \sigma_e}{\partial \sigma_\theta}\frac{\partial \sigma_\theta}{\partial \mathbf{q}} + \frac{\partial \sigma_e}{\partial \sigma_z}\frac{\partial \sigma_z}{\partial \mathbf{q}} + \frac{\partial \sigma_e}{\partial \tau_{rz}}\frac{\partial \tau_{rz}}{\partial \mathbf{q}}, \tag{38}$$

where

$$\frac{\partial \sigma_e}{\partial \sigma_r} = \frac{2\sigma_r - \sigma_\theta - \sigma_z}{2\sqrt{\sigma_e}}, \tag{39}$$

$$\frac{\partial \sigma_e}{\partial \sigma_\theta} = \frac{2\sigma_\theta - \sigma_r - \sigma_z}{2\sqrt{\sigma_e}}, \tag{40}$$

$$\frac{\partial \sigma_e}{\partial \sigma_z} = \frac{2\sigma_z - \sigma_r - \sigma_\theta}{2\sqrt{\sigma_e}}, \tag{41}$$

$$\frac{\partial \sigma_e}{\partial \tau_{rz}} = \frac{6\tau_{rz}}{2\sqrt{\sigma_e}}. \tag{42}$$

2.6. Displacement constraints

Displacement and von Mises stress constraints can be applied anywhere in the die. In this work, two displacement constraints have been selected and these have been applied near the casting where the y and x-displacements have been set not to exceed 1×10^{-4} m applied at points F and G, respectively. These have been chosen to avoid high displacements at the casting, which are typically the crucial areas in which the high von Mises stress are developed and as a consequence, failure initiation might occur. Fig. 7 shows the application points for the two displacement constraints in the die.

2.7. Shape design element

The Design Element Concept is not only applicable to parameter sensitivity, it can also be applied to shape sensitivity. In this section, a new and novel application of shape design element of coolant channels is demonstrated. Shape sensitivity can to some extent be applied to part shape design, but often this is driven by end application considerations. In this work it may be applied to process design through for example positioning of the cooling system within the die. This will be explored within the case studies that will be considered in this project. However, in the following case studies, the coolant channel

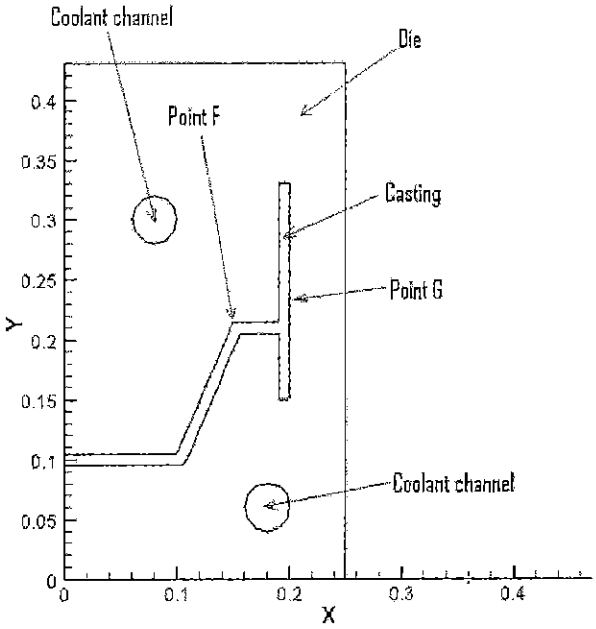

Fig. 7. Application of displacement and von Mises stress constraints.

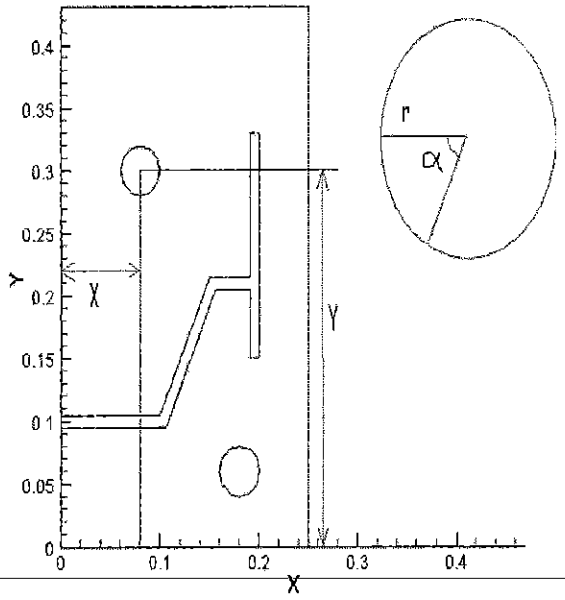

Fig. 8. The definition of X and Y coordinates of the centre of the coolant channels.

was not moved around, it was just the case of showing how the sensitivity of the chosen position will respond with respect to the application of the von Mises stress constraint.

2.7.1. Shape parameterisation of coolant channel

One of the important aspects in performing shape sensitivities for coolant channel geometry is the parameterisation of the coolant channel. To illustrate this, Fig. 3 shows the X and Y coordinates of the coolant channel centre. The shape sensitivities with respect to the X and Y coordinates are calculated after parameterisation and the von Mises stress constraints have been applied at points F and G as shown in Fig. 8. These have been chosen due to the high von Mises stress values in these areas. The parameterisation of the coolant channels is as follows:

$$x = X - r\cos\alpha,$$
$$y = Y - r\sin\alpha,$$

where r is the radius of the coolant channel and α is the angle as shown in Fig. 8.

2.7.2. The stiffness matrix derivative for shape sensitivities

Again, in performing analytical design element shape sensitivity analysis, the success of the computation is largely dependent on the calculated stiffness matrix derivative. Thus, for an axi-symmetric problem, the derivative of the stiffness matrix with respect to the design variable, associated with the Y-coordinate of the centre of the coolant channel, is given as:

$$\frac{\partial \mathbf{K}}{\partial \mathbf{Y}} = \left(\frac{\partial \mathbf{B}^T}{\partial \mathbf{Y}} D\mathbf{B}\mathbf{J}_D + \mathbf{B}^T D \frac{\partial \mathbf{B}}{\partial \mathbf{Y}} \mathbf{J}_D + \mathbf{B}^T D\mathbf{B} \frac{\partial \mathbf{J}_D}{\partial \mathbf{Y}} \right) \pi \mathbf{r}_{bar}. \tag{43}$$

The derivative of the stiffness matrix with respect to the X-coordinate of the centre of the coolant channel is of the form,

$$\frac{\partial \mathbf{K}}{\partial \mathbf{X}} = \left(\frac{\partial \mathbf{B}^T}{\partial \mathbf{X}} D\mathbf{B}\mathbf{J}_D \mathbf{r}_{bar} + \mathbf{B}^T D \frac{\partial \mathbf{B}}{\partial \mathbf{X}} \mathbf{J}_D \mathbf{r}_{bar} + \mathbf{B}^T D\mathbf{B} \frac{\partial \mathbf{J}_D}{\partial \mathbf{X}} \mathbf{r}_{bar} + \mathbf{B}^T D\mathbf{B}\mathbf{J}_D \frac{\partial \mathbf{r}_{bar}}{\partial \mathbf{X}} \right) \pi. \tag{44}$$

3. Parameter design element sensitivities example

The design sensitivity analysis example of the axi-symmetric squeeze formed wheel is presented. The thermal stress analysis requires a temperature prescription within the die as an input and this was derived from a thermal analysis using the procedure that has been described fully in previous section. In this instance, the initial temperature of the cast metal was 700 °C. The cast material is Aluminium LM25 whereas for the die, the material is steel H13. The die features two coolant channels that are fixed in position and it has an initial temperature of 200 °C [33]. The heat transfer conditions in the coolant system corresponds to a heat transfer coefficient and reference temperature of 1000 W/m^2 K (Appendix II) and 100 °C respectively and heat is removed from the external surfaces in accordance with a heat transfer coefficient to 25 W/m^2 K [29,34] and an ambient temperature of 25 °C. Very good contact is assumed at the die and casting interface, hence an interfacial coefficient of 5000 W/m^2 K [34,35] was applied.

3.1. Transient thermo-mechanical problem

Fig. 9 shows the temperature field in the die at $t = 50$ s after the cast part has completely solidified. At $t = 50$ s, the temperature field in the die was directly used for the calculation of thermal stresses for the structural evaluation. Figs. 10–12 show the x-displacement, y-displacement and von Mises stress in the die at $t = 50$ s. The range of x and y displacements is 10^{-4} m and 10^8 Pa for von Mises stress. The temperature distribution in the die leads to a complex stress pattern where high von Mises stresses are developed near the coolant channels and also in the corner regions within the die.

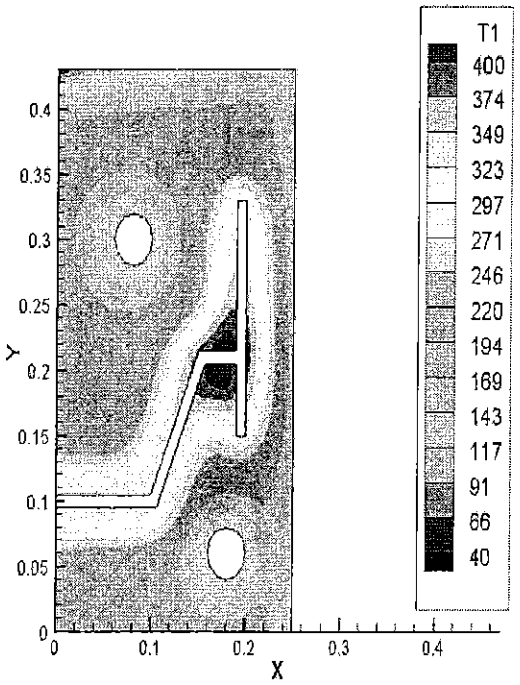

Fig. 9. Temperature field in the die at $t = 50$ s.

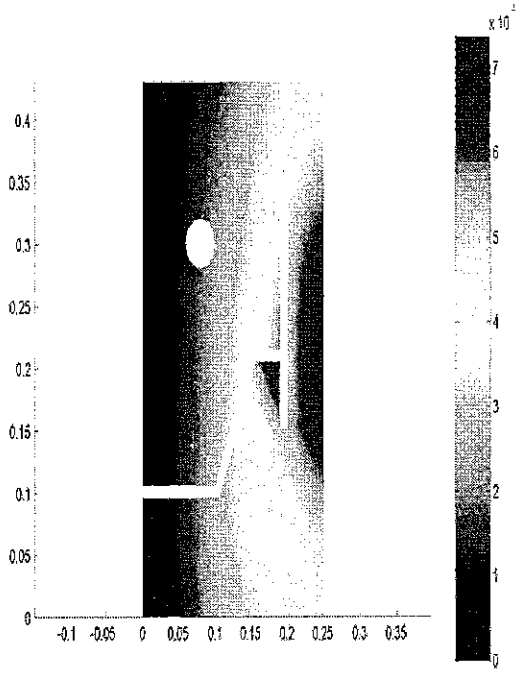

Fig. 10. *X*-displacement in the die at $t = 50$ s.

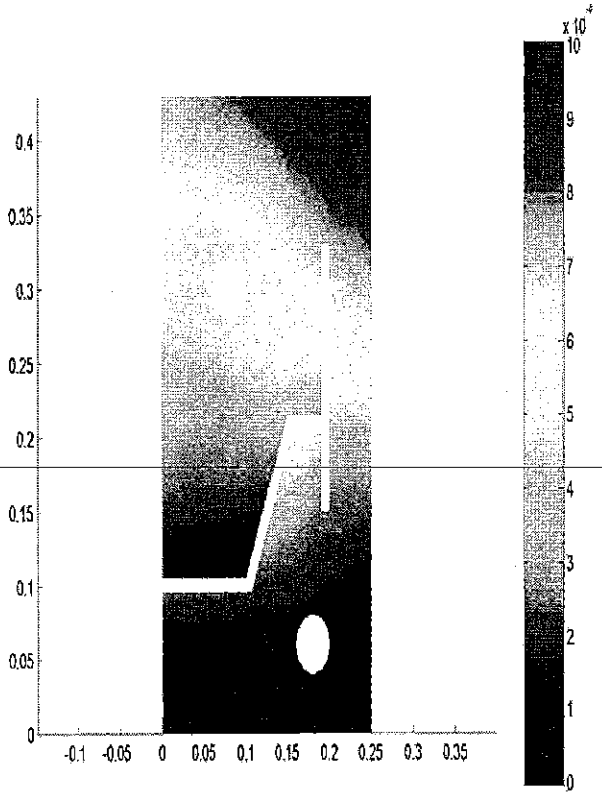

Fig. 11. *Y*-displacement in the die at $t = 50$ s.

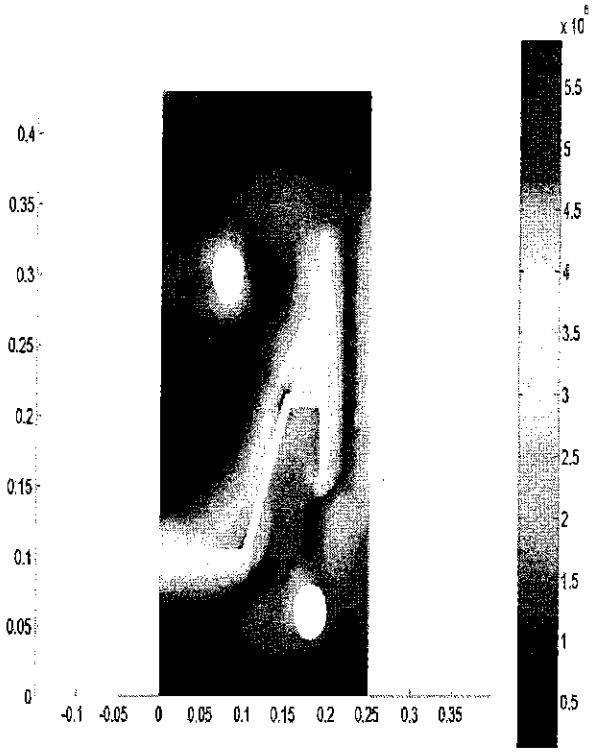

Fig. 12. Von Mises stress distribution in the die at $t = 50$ s.

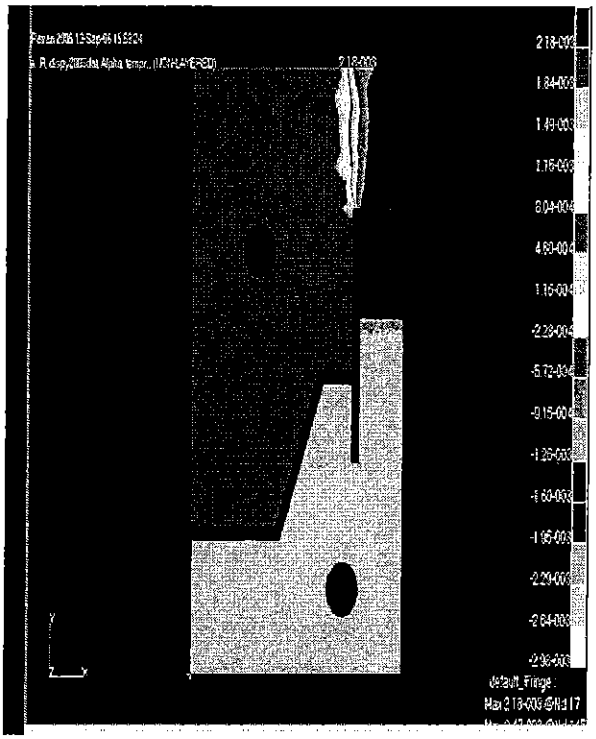

Fig. 13. Design element sensitivity of displacement with respect to Young modulus for the application of displacement constraint at point F for 3 design elements.

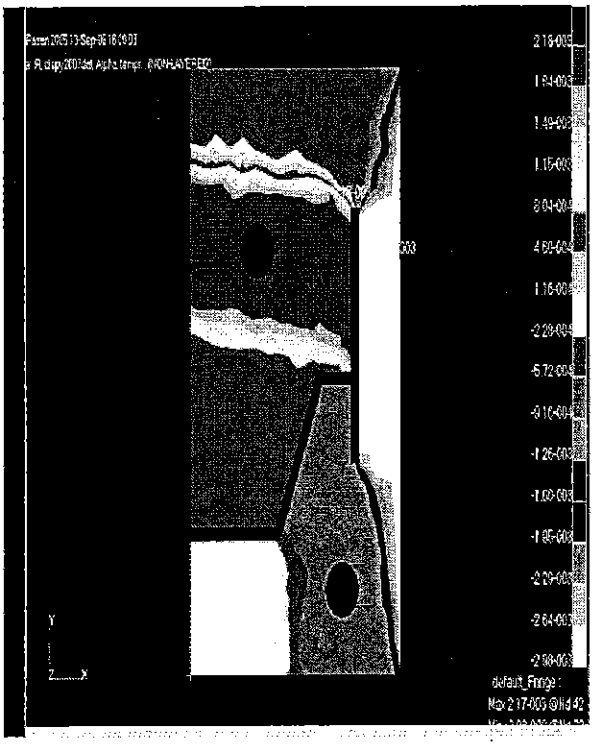

Fig. 14. Design element sensitivity of displacement with respect to Young modulus for the application of displacement constraint at point F for 7 design elements.

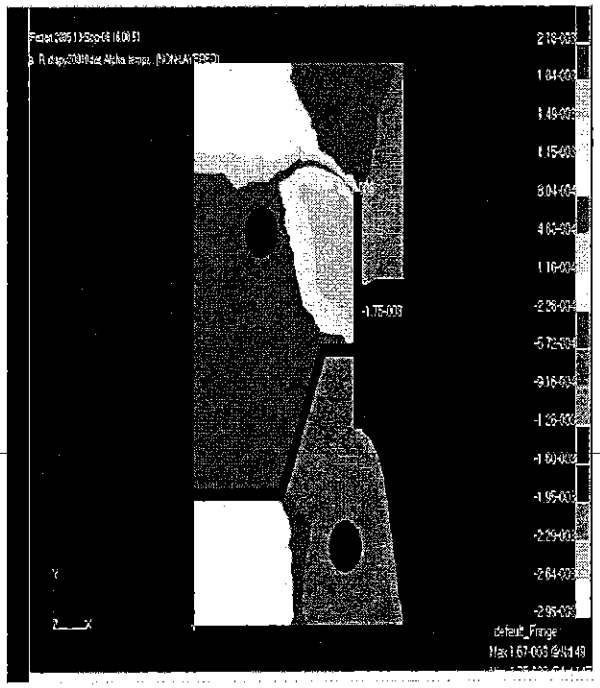

Fig. 15. Design element sensitivity of displacement with respect to Young modulus for the application of displacement constraint at point F for 10 design elements.

3.2. Displacement design element sensitivities

The same points for the application of design constraints as in the previous section have been applied. In implementation, there are a number of design element subdivisions that may be used, for example, each block in the die may be a design

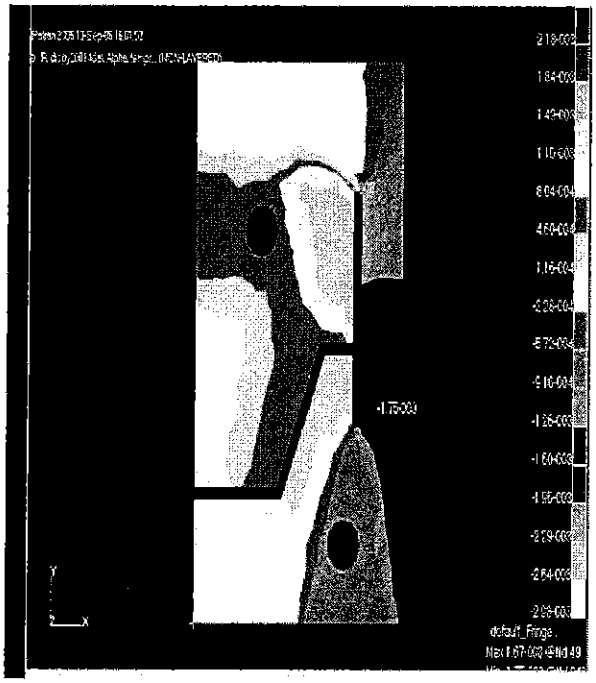

Fig. 16. Design element sensitivity of displacement with respect to Young modulus for the application of displacement constraint at point F for 14 design elements.

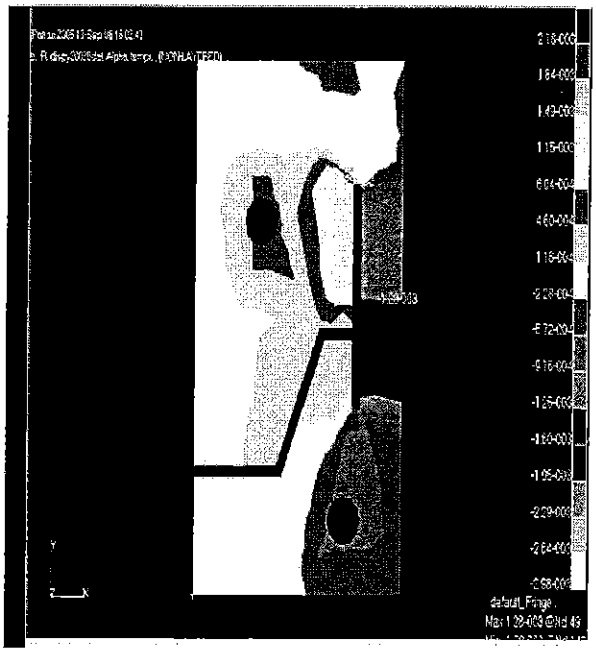

Fig. 17. Design element sensitivity of displacement with respect to Young modulus for the application of displacement constraint at point F for 28 design elements

element. This will lead to just a few design elements and these may be insufficient to capture stress or thermal gra dients within the die with sufficient accuracy. Thus a number of design element subdivisions will be explored and the o ptions are presented in Figs. 2–6.

Figs. 13–17 show the design element sensitivity of displacement with respect to Young modulus for the application of the displacement constraint at locations F for 3, 7, 10, 14 and 28 design elements respectively. Figs. 18–22 show the design element sensitivity of displacement with respect to Young modulus for the application of the displacement constraint at

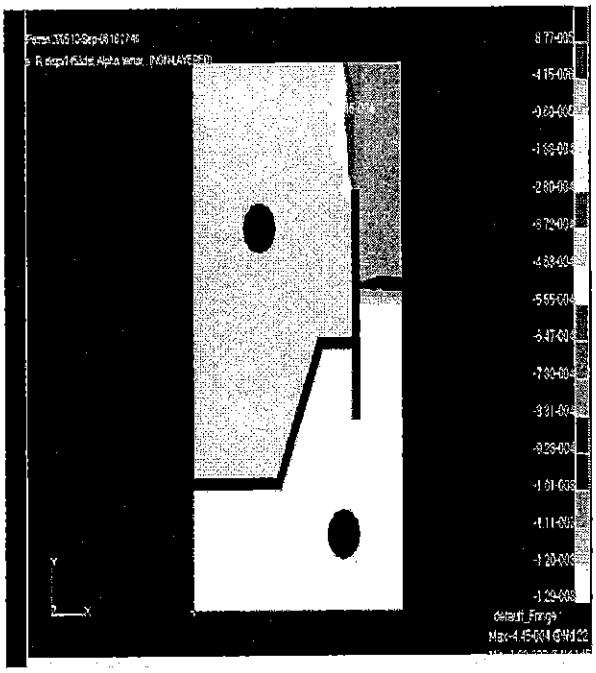

Fig. 18. Design element sensitivity of displacement with respect to Young modulus for the application of displacement constraint at point G for 3 design elements.

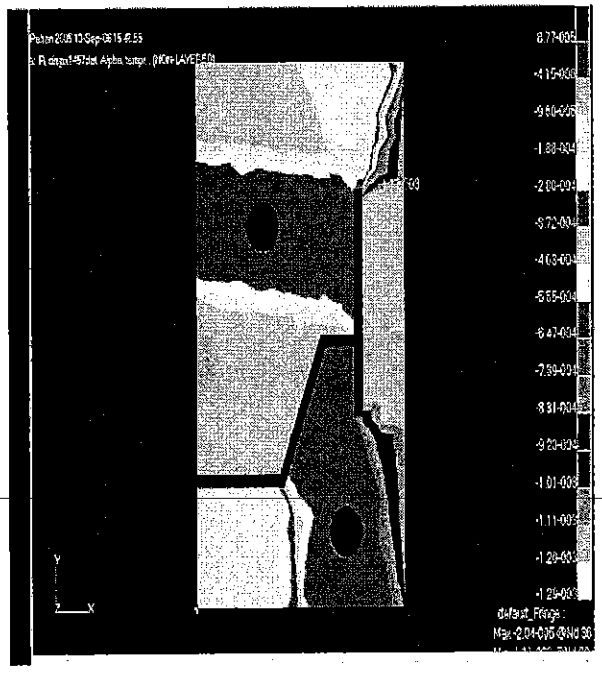

Fig. 19. Design element sensitivity of displacement with respect to Young modulus for the application of displacement constraint at point G for 7 design elements.

locations G for 3, 7, 10, 14 and 28 design elements respectively. It can be seen that for the results obtained for both displacement constraints, the division of design elements affected the sensitivity distribution in the die and convergence can be observed as more design elements are employed.

At the finite element level, all the calculated sensitivities using the analytical methods may be compared with the FDM method to ensure the accuracy of the calculated sensitivities. In terms of validation of the approach in this work involving the sensitivities for the Design Element Concept, the same procedure has been implemented where all the calculated design

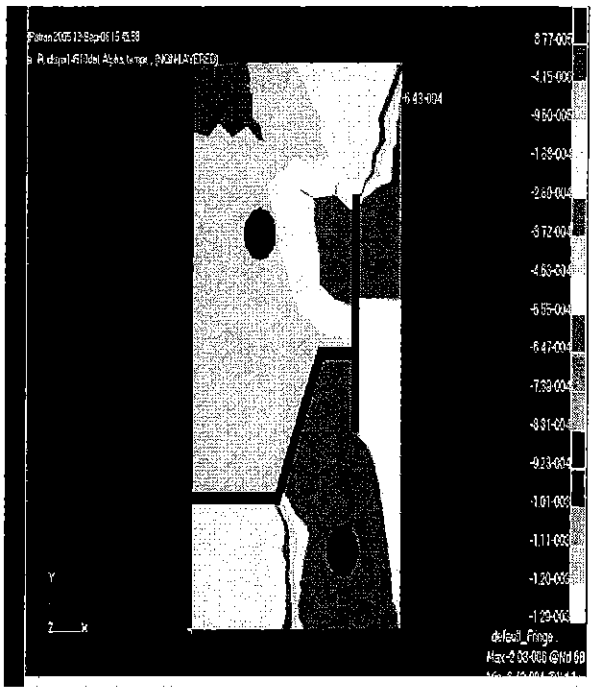

Fig. 20. Design element sensitivity of displacement with respect to Young modulus for the application of displacement constraint at point G for 10 design elements.

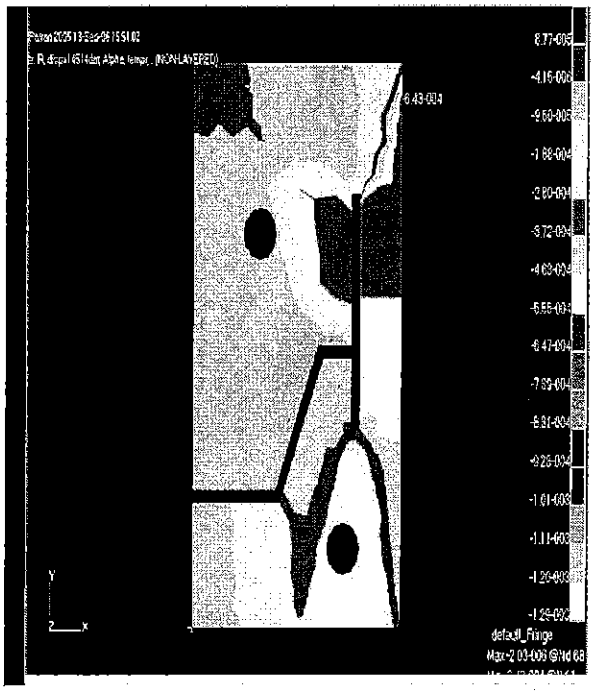

Fig. 21. Design element sensitivity of displacement with respect to Young modulus for the application of displacement constraint at point G for 14 design elements.

element sensitivities using analytical methods will be compared with the FDM method. This is now practical since the Design Element Concept is a macro scale sensitivity of the FE sensitivities as discussed in the previous sections. The comparison of the results between the two methods was carried out and it is effectively a validation loop, where the results showed close agreement. The comparison was done for the patterns obtained from both, the AVM and the DDM solutions, where they were compared with the pattern obtained from the FDM solutions.

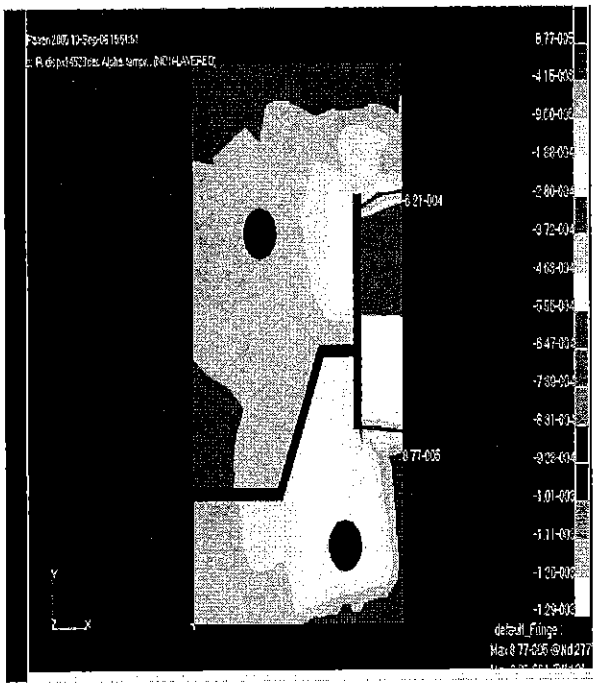

Fig. 22. Design element sensitivity of displacement with respect to Young modulus for the application of displacement constraint at point G for 28 design elements.

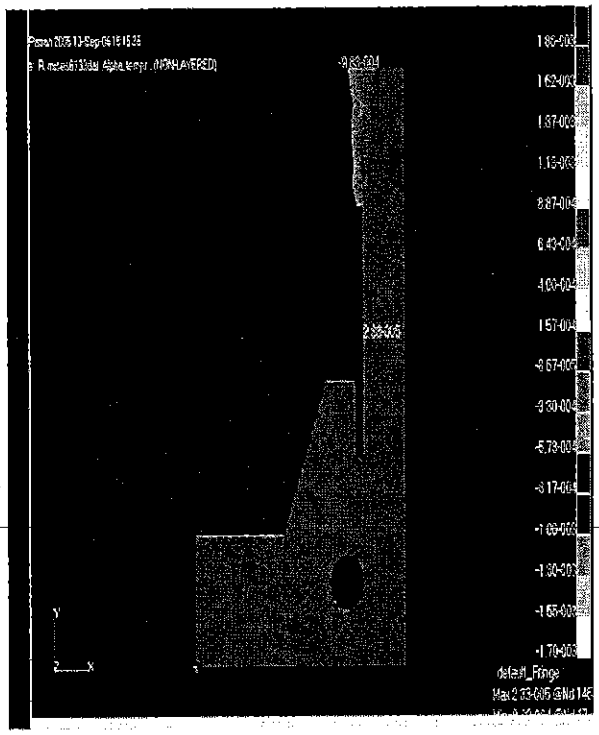

Fig. 23. Design element sensitivity of von Mises stress with respect to Young modulus for the application of von Mises stress constraint at point F for 3 design elements.

3.3. Von Mises stress design element sensitivities

The same points for the application of von Mises stress constraints as defined in the previous section have been applied where the von Mises stress has been set not to exceed 1×10^8 Pa. This has been chosen due to the high von Mises stress values in these areas. Figs. 23–27 show the design element sensitivity of von Mises stress with respect to Young modulus

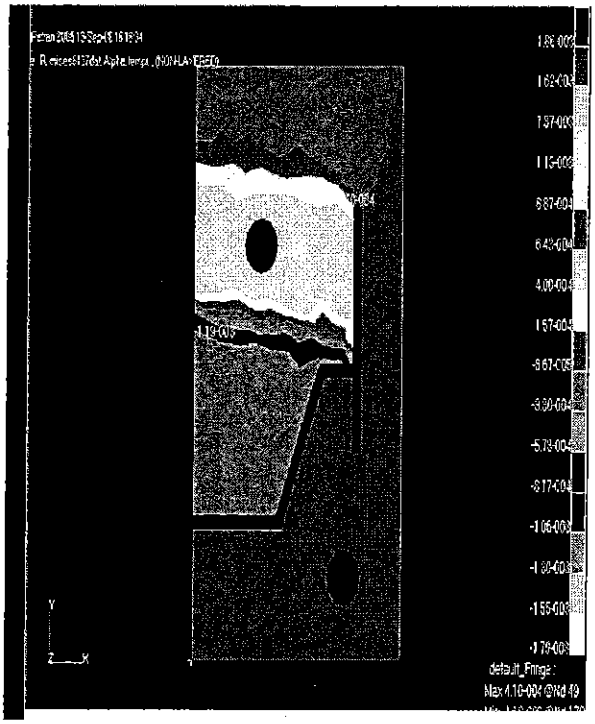

Fig. 24. Design element sensitivity of von Mises stress with respect to Young modulus for the application of von Mises stress constraint at point F for 7 design elements.

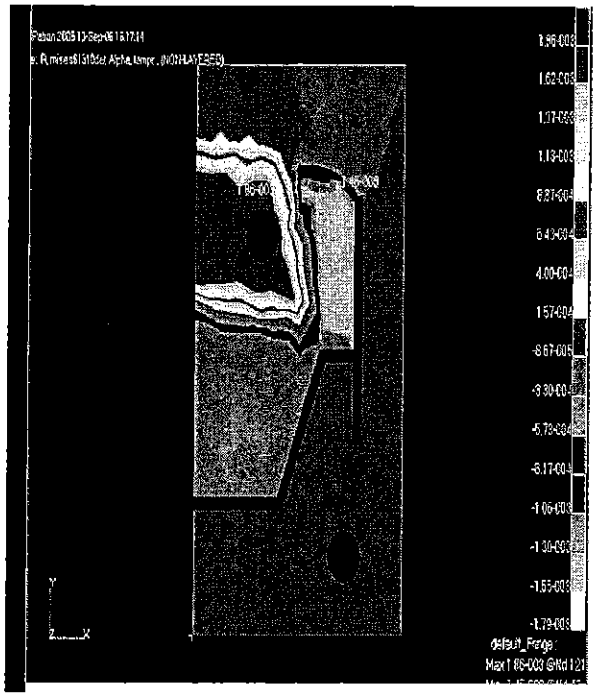

Fig. 25. Design element sensitivity of von Mises stress with respect to Young modulus for the application of von Mises stress constraint at point F for 10 design elements.

for the application of von Mises stress constraint at points F for 3, 7, 10, 14 and 28 design elements respectively. Figs. 28–32 show the design element sensitivity of von Mises stress with respect to Young modulus for the application of von Mises stress constraint at points G for 3, 7, 10, 14 and 28 design elements respectively. Again, for von Mises stress

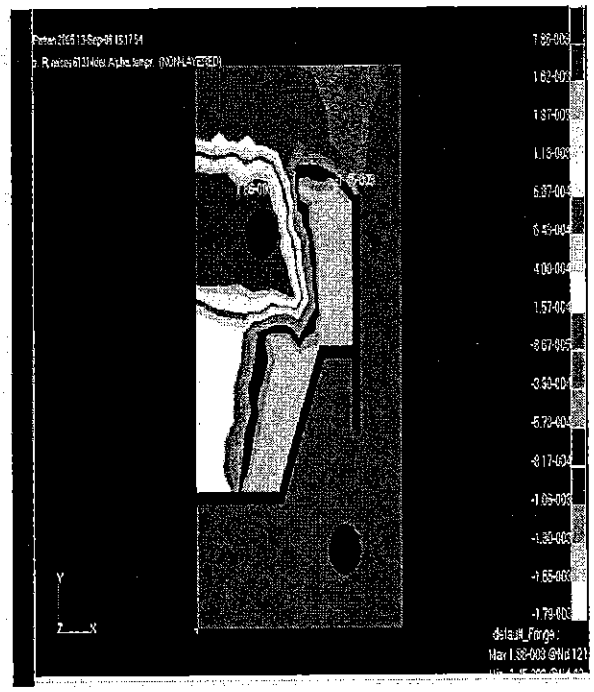

Fig. 26. Design element sensitivity of von Mises stress with respect to Young modulus for the application of von Mises stress constraint at point F for 14 design elements.

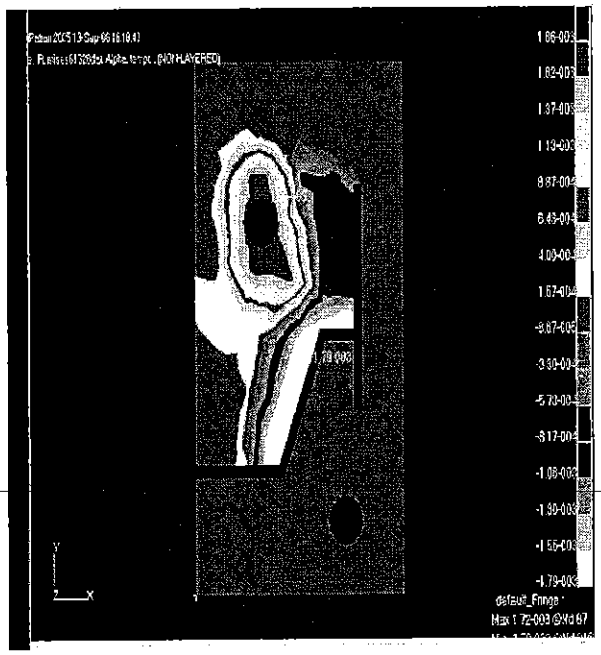

Fig. 27. Design element sensitivity of von Mises stress with respect to Young modulus for the application of von Mises stress constraint at point F for 28 design elements.

constraints, it can be seen that as more design elements are explored, convergence is obtained as shown by Figs. 23–27 and 28–32.

Clearly the Design Element for both displacement and von Mises stress have tremendously reduced the number of design variables. The reduction of the design variables from hundreds to only a few design elements has reduced the calculation time in the optimisation process by a factor of more than ten times since the updating of new solution using the gradient-based optimisation is done accordingly for each design variable. This is due to the fact that the gradient-based

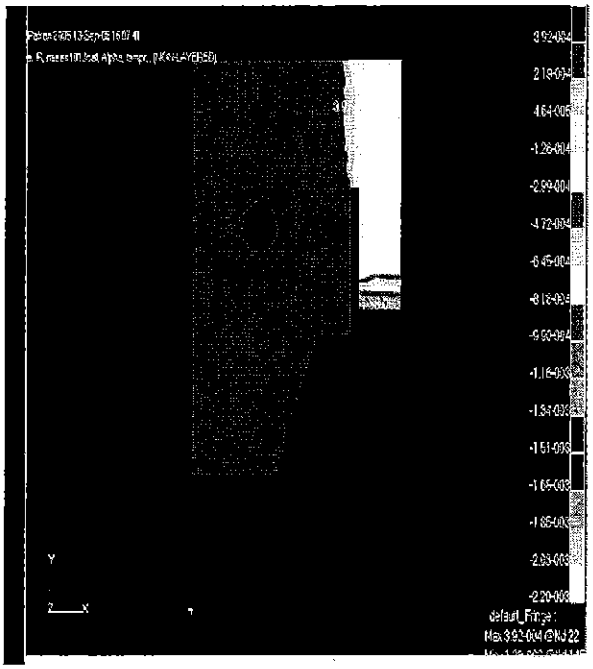

Fig. 28. Design element sensitivity of von Mises stress with respect to Young modulus for the application of von Mises stress constraint at point G for 3 design elements.

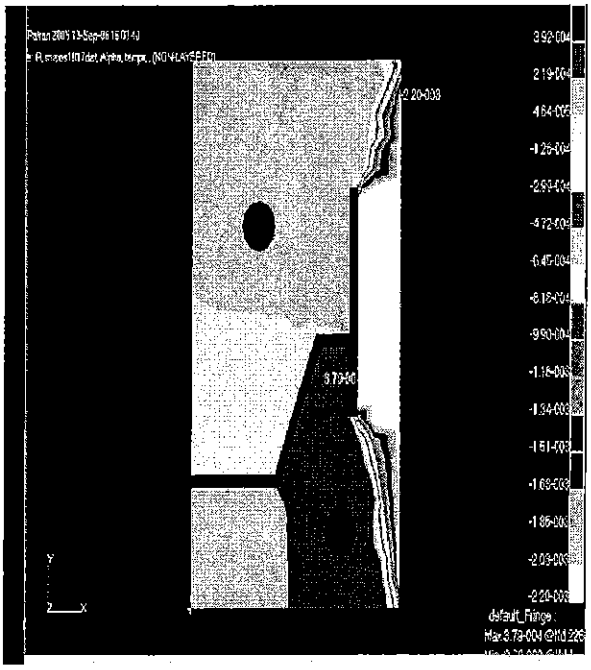

Fig. 29. Design element sensitivity of von Mises stress with respect to Young modulus for the application of von Mises stress constraint at point G for 7 design elements.

optimisation updates the new solution based on the Taylor series formulation, where the sensitivity with respect to each design variable is needed in deriving to the optimal solution.

3.4. Analytical methods vs finite difference method

In this section, the calculated analytical design element sensitivity gradients are tabulated and then compared with the results from a simple difference based calculation. In this section only a limited comparison is presented, because good agreement was shown for all cases.

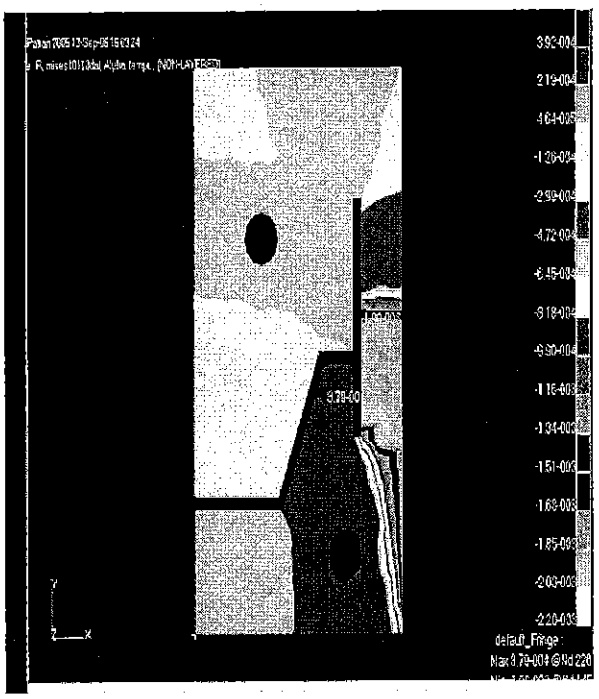

Fig. 30. Design element sensitivity of von Mises stress with respect to Young modulus for the application of von Mises stress constraint at point G for 10 design elements.

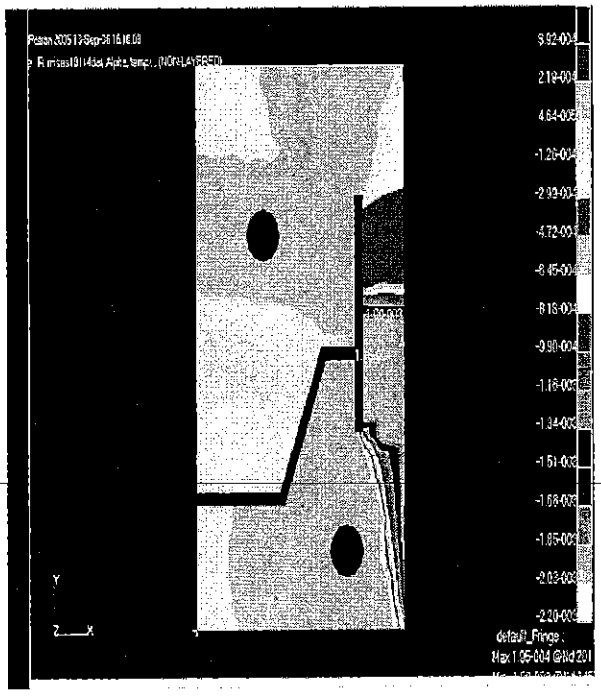

Fig. 31. Design element sensitivity of von Mises stress with respect to Young Modulus for the application of von Mises stress constraint at point G for 14 design elements.

3.4.1. Design element sensitivities of displacement

Tables 1 and 2 show the design element sensitivities of displacement with respect to the Young modulus for the application of displacement constraints at points F and G respectively for 14 design elements. The results are tabulated up to three decimal places due to the fairly close values that were obtained from the FDM and the analytical methods.

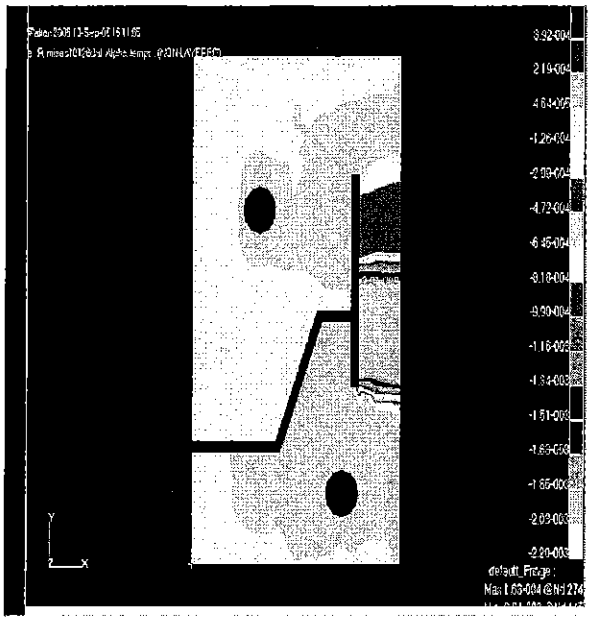

Fig. 32. Design element sensitivity of von Mises stress with respect to Young Modulus for the application of von Mises stress constraint at point G for 28 design elements.

Table 1
Comparison of the analytical methods and FDM design derivatives for the application of displacement constraint at point F for 14 design elements.

Design element	FDM (F)				FDM (C)				AVM and DDM
	0.2%	% Error	2.0%	% Error	0.2%	% Error	2.0%	% Error	
1	2.371×10^{-15}	0.78	2.439×10^{-15}	2.05	2.389×10^{-15}	0.04	2.369×10^{-15}	0.88	2.390×10^{-15}
2	1.689×10^{-14}	0.23	1.710×10^{-14}	1.42	1.687×10^{-14}	0.08	1.698×10^{-14}	0.71	1.686×10^{-14}
3	4.949×10^{-14}	0.67	5.029×10^{-14}	0.94	4.982×10^{-14}	2.01×10^{-3}	4.951×10^{-14}	0.62	4.982×10^{-14}
4	2.177×10^{-14}	0.17	2.201×10^{-14}	1.29	2.173×10^{-14}	0.02	2.173×10^{-14}	0.92	2.173×10^{-14}
5	1.416×10^{-13}	0.28	1.433×10^{-13}	0.92	1.419×10^{-13}	0.12	1.411×10^{-13}	0.59	1.421×10^{-13}
6	1.867×10^{-13}	0.79	1.909×10^{-13}	1.47	1.882×10^{-13}	0.03	1.886×10^{-13}	0.21	1.882×10^{-13}
7	-8.833×10^{-13}	0.56	-8.868×10^{-13}	0.17	-8.882×10^{-13}	2.25×10^{-3}	-8.889×10^{-13}	0.07	-8.883×10^{-13}
8	-9.559×10^{-13}	0.09	-9.560×10^{-13}	0.08	-9.568×10^{-13}	5.22×10^{-3}	-9.576×10^{-13}	0.07	-9.569×10^{-13}
9	-5.200×10^{-13}	0.5	-5.171×10^{-13}	0.05	-5.172×10^{-13}	0.04	-5.171×10^{-13}	0.05	-5.174×10^{-13}
10	-5.051×10^{-13}	0.98	-5.097×10^{-13}	0.11	-5.101×10^{-13}	0.01	-5.103×10^{-13}	0.02	-5.102×10^{-13}
11	1.854×10^{-11}	0.31	1.856×10^{-11}	0.19	1.858×10^{-11}	0.07	1.858×10^{-11}	0.05	1.859×10^{-11}
12	-1.436×10^{-11}	0.97	-1.442×10^{-11}	0.55	-1.452×10^{-11}	0.14	-1.451×10^{-11}	0.07	-1.450×10^{-11}
13	1.925×10^{-12}	0.47	1.935×10^{-12}	0.05	1.934×10^{-12}	5.16×10^{-3}	1.934×10^{-12}	5.16×10^{-3}	1.934×10^{-12}
14	-1.375×10^{-11}	0.93	-1.379×10^{-11}	0.63	-1.390×10^{-11}	0.14	-1.388×10^{-11}	0.07	-1.388×10^{-11}

3.4.2. Design element sensitivities von Mises stress

Tables 3 and 4 show the design element sensitivities of von Mises stress with respect to the Young modulus for the application of von Mises stress constraints at point F and G respectively for 14 design elements.

From this tabulation, it can be seen that the results showed close agreement. It reflects the results obtained for the comparison done for the full field solution from the AVM and the DDM, where again, the percentage errors obtained were also small.

3.5. Shape Design Element Concept example

This section will highlight the influence of the tendency of the movement of the coolant channel having a radius of 0.02 m in certain directions, for instance X and Y axis, with respect to the von Mises stress constraint at a particular point in the die. The same initial and boundary conditions were applied as described previously. Tables 5 and 6 show the design element sensitivities of von Mises stress with respect to Y and X coordinates for the lower coolant channel for the application of the von Mises stress constraint at point F. It can be seen that the tendency to move the lower coolant channel in the X-direction has a higher influence than the Y-direction with respect to the von Mises stress constraint at point F. Tables 7 and 8 show the

Table 2
Comparison of the analytical methods and FDM design derivatives for the application of displacement constraint at point G for 14 design elements.

Design element	FDM (F)				FDM (C)				AVM and DDM
	0.2%	% Error	2.0%	% Error	0.2%	% Error	2.0%	% Error	
1	2.246×10^{-13}	0.94	2.238×10^{-13}	0.56	2.225×10^{-13}	0.03	2.240×10^{-13}	0.67	2.225×10^{-13}
2	1.112×10^{-12}	0.63	1.090×10^{-12}	1.32	1.101×10^{-12}	0.36	1.112×10^{-12}	0.63	1.105×10^{-12}
3	1.934×10^{-12}	0.56	1.942×10^{-12}	1.03	1.945×10^{-12}	$1.03 \times 10{-}3$	1.932×10^{-12}	0.67	1.945×10^{-12}
4	1.871×10^{-12}	1.29	1.835×10^{-12}	0.65	1.843×10^{-12}	0.16	1.842×10^{-12}	0.26	1.847×10^{-12}
5	-1.887×10^{-11}	0.4	-1.868×10^{-11}	1.14	-1.896×10^{-11}	0.08	-1.896×10^{-11}	0.08	-1.895×10^{-11}
6	-2.993×10^{-12}	0.43	-2.981×10^{-12}	0.83	-3.005×10^{-12}	0.02	-2.997×10^{-12}	0.07	-3.006×10^{-12}
7	1.245×10^{-12}	1.38	1.216×10^{-12}	0.98	1.230×10^{-12}	0.14	1.216×10^{-12}	0.96	1.228×10^{-12}
8	7.941×10^{-13}	0.15	7.862×10^{-13}	1.14	7.943×10^{-13}	0.12	7.902×10^{-13}	0.64	7.953×10^{-13}
9	6.114×10^{-13}	0.82	6.069×10^{-13}	0.41	6.102×10^{-13}	0.13	6.130×10^{-13}	0.58	6.094×10^{-13}
10	3.471×10^{-13}	0.84	3.435×10^{-13}	0.2	3.445×10^{-13}	0.08	3.474×10^{-13}	0.93	3.442×10^{-13}
11	6.436×10^{-13}	0.68	6.358×10^{-13}	0.55	6.404×10^{-13}	0.17	6.426×10^{-13}	0.52	6.393×10^{-13}
12	1.506×10^{-12}	1.27	1.475×10^{-12}	0.79	1.488×10^{-12}	0.1	1.502×10^{-12}	0.98	1.487×10^{-12}
13	4.635×10^{-14}	0.07	4.607×10^{-14}	0.68	4.617×10^{-14}	0.46	4.638×10^{-14}	2.15×10^{-3}	4.638×10^{-14}
14	-2.613×10^{-15}	0.53	-2.601×10^{-15}	0.99	-2.629×10^{-15}	0.05	-2.624×10^{-15}	0.12	-2.627×10^{-15}

Table 3
Comparison of the analytical methods and FDM design derivatives for the application of von Mises stress constraint at point F for 14 design elements.

Design element	FDM (F)				FDM (C)				AVM and DDM
	0.2%	% Error	2.0%	% Error	0.2%	% Error	2.0%	% Error	
1	3.292×10^{-14}	0.51	3.280×10^{-14}	0.88	3.306×10^{-14}	0.09	3.296×10^{-14}	0.39	3.309×10^{-14}
2	-1.965×10^{-13}	0.67	-1.972×10^{-13}	1.02	-1.956×10^{-13}	0.20	-1.961×10^{-13}	0.46	-1.952×10^{-13}
3	1.834×10^{-12}	0.65	1.845×10^{-12}	1.26	1.819×10^{-12}	0.16	1.812×10^{-12}	0.55	1.822×10^{-12}
4	-8.846×10^{-12}	0.48	-8.818×10^{-12}	0.79	-8.909×10^{-12}	0.22	-8.852×10^{-12}	0.41	-8.889×10^{-12}
5	-1.734×10^{-11}	0.63	-1.731×10^{-11}	0.80	-1.750×10^{-11}	0.29	-1.754×10^{-11}	0.52	-1.745×10^{-11}
6	-1.225×10^{-11}	0.56	-1.219×10^{-11}	1.05	-1.232×10^{-11}	0.07	-1.226×10^{-11}	0.48	-1.232×10^{-11}
7	-2.326×10^{-12}	0.68	-2.320×10^{-12}	0.94	-2.338×10^{-12}	0.17	-2.356×10^{-12}	0.59	-2.342×10^{-12}
8	-1.916×10^{-12}	0.57	-1.909×10^{-12}	0.93	-1.929×10^{-12}	0.10	-1.936×10^{-12}	0.47	-1.927×10^{-12}
9	-1.577×10^{-12}	0.57	-1.569×10^{-12}	1.07	-1.583×10^{-12}	0.19	-1.578×10^{-12}	0.50	-1.586×10^{-12}
10	-1.605×10^{-12}	0.86	-1.610×10^{-12}	0.55	-1.612×10^{-12}	0.43	-1.620×10^{-12}	0.06	-1.619×10^{-12}
11	5.023×10^{-12}	0.63	5.032×10^{-12}	0.82	5.001×10^{-12}	0.22	5.015×10^{-12}	0.48	4.991×10^{-12}
12	1.662×10^{-11}	0.54	1.683×10^{-11}	0.72	1.675×10^{-11}	0.28	1.679×10^{-11}	0.47	1.671×10^{-11}
13	4.466×10^{-13}	0.58	4.490×10^{-13}	0.04	4.484×10^{-13}	0.2	4.494×10^{-13}	0.02	4.493×10^{-13}
14	4.780×10^{-12}	0.27	4.758×10^{-12}	0.19	4.769×10^{-12}	0.04	4.768×10^{-12}	0.02	4.767×10^{-12}

Table 4
Comparison of the analytical methods and FDM design derivatives for the application of von Mises stress constraint at point G for 14 design elements.

Design element	FDM (F)				FDM (C)				AVM and DDM
	0.2%	% Error	2.0%	% Error	0.2%	% Error	2.0%	% Error	
1	-2.459×10^{-13}	0.32	-2.480×10^{-13}	0.53	-2.469×10^{-13}	0.08	-2.463×10^{-13}	0.16	-2.467×10^{-13}
2	-1.573×10^{-12}	0.19	-1.565×10^{-12}	0.69	-1.575×10^{-12}	0.06	-1.570×10^{-12}	0.38	-1.576×10^{-12}
3	-4.156×10^{-12}	0.72	-4.211×10^{-12}	0.60	-4.187×10^{-12}	0.02	-4.181×10^{-12}	0.12	-4.186×10^{-12}
4	-2.197×10^{-12}	0.32	-2.218×10^{-12}	0.59	-2.207×10^{-12}	0.09	-2.213×10^{-12}	0.36	-2.205×10^{-12}
5	-4.633×10^{-12}	0.30	-4.670×10^{-12}	0.49	-4.642×10^{-12}	0.11	-4.636×10^{-12}	0.24	-4.647×10^{-12}
6	-6.396×10^{-12}	0.48	-6.462×10^{-12}	0.54	-6.431×10^{-12}	0.06	-6.457×10^{-12}	0.47	-6.427×10^{-12}
7	-1.251×10^{-12}	0.40	-1.255×10^{-12}	0.72	-1.248×10^{-12}	0.16	-1.242×10^{-12}	0.32	-1.246×10^{-12}
8	-3.465×10^{-13}	0.23	-3.471×10^{-13}	0.40	-3.456×10^{-13}	0.03	-3.451×10^{-13}	0.17	-3.457×10^{-13}
9	-1.851×10^{-13}	0.48	-1.856×10^{-13}	0.76	-1.840×10^{-13}	0.11	-1.849×10^{-13}	0.38	-1.842×10^{-13}
10	-2.032×10^{-14}	0.30	-2.038×10^{-14}	0.59	-2.029×10^{-14}	0.15	-2.021×10^{-14}	0.25	-2.026×10^{-14}
11	-8.080×10^{-13}	0.26	-8.096×10^{-13}	0.46	-8.055×10^{-13}	0.05	-8.036×10^{-13}	0.29	-8.059×10^{-13}
12	-2.810×10^{-12}	0.71	-2.853×10^{-12}	0.81	-2.838×10^{-12}	0.28	-2.843×10^{-12}	0.50	-2.830×10^{-12}
13	-9.200×10^{-14}	0.96	-9.283×10^{-14}	0.06	-9.350×10^{-14}	0.65	-9.288×10^{-14}	0.01	-9.289×10^{-14}
14	-1.649×10^{-13}	1.02	-1.664×10^{-13}	0.12	-1.667×10^{-13}	0.06	-1.667×10^{-13}	0.06	-1.666×10^{-13}

design element sensitivities of von Mises stress with respect to Y and X coordinates of the lower coolant channel for the application of von Mises stress constraint at point G. However, from these results, the tendency to move the lower coolant channel in the Y-direction has a higher influence than the X-direction with respect to the von Mises stress constraint at point G.

Table 5
The design element sensitivities of von Mises stress with respect to Y coordinate of the lower coolant channel for the application of von Mises stress constraint at point F.

	dSe/de (1×10^{-4})
AVM and DDM	8.759

	% Perturb	dSe/de (1×10^{-4})	% Error
FDM (C)	0.2	8.759	8.52×10^{-4}
FDM (C)	2	8.765	0.07

Table 6
The design element sensitivities of von Mises stress with respect to X coordinate of the lower coolant channel for the application of von Mises stress constraint at point F.

	dSe/de (1×10^{-3})
AVM and DDM	−1.332

	% Perturb	dSe/de (1×10^{-3})	% Error
FDM (C)	0.2	−1.331	0.02
FDM (C)	2	−1.302	2.27

Table 7
The design element sensitivities of von Mises stress with respect to Y coordinate of the lower coolant channel for the application of von Mises stress constraint at point G.

	dSe/de (1×10^{-1})
AVM and DDM	−2.670

	% Perturb	dSe/de (1×10^{-1})	% Error
FDM (C)	0.2	−2.670	3.12×10^{-4}
FDM (C)	2	−2.669	0.02

Table 8
The design element sensitivities of von Mises stress with respect to X coordinate of the lower coolant channel for the application of von Mises stress constraint at point G.

	dSe/de (1×10^{-2})
AVM and DDM	−6.368

	% Perturb	dSe/de (1×10^{-2})	% Error
FDM (C)	0.2	−6.368	2.97×10^{-3}
FDM (C)	2	−6.385	0.27

Table 9
The design element sensitivities of von Mises stress with respect to Y coordinate of the upper coolant channel for the application of von Mises stress constraint at point F.

	dSe/de (1×10^{-1})
AVM and DDM	−5.799

	% Perturb	dSe/de (1×10^{-1})	% Error
FDM (C)	0.2	−5.799	1.84×10^{-3}
FDM (C)	2	−5.809	0.17

Tables 9 and 10 show the design element sensitivities of von Mises stress with respect to Y and X coordinates of the upper coolant channel for the application of von Mises stress constraint at point F. Tables 11 and 12 show the design element

Table 10
The design element sensitivities of von Mises stress with respect to X coordinate of the upper coolant channel for the application of von Mises stress constraint at point F.

			dSe/de (1×10^{-2})
AVM and DDM			−1.792
	% Perturb	dSe/de (1×10^{-2})	% Error
FDM (C)	0.2	−1.792	5.3×10^{-4}
FDM (C)	2	−1.791	0.05

Table 11
The design element sensitivities of von Mises stress with respect to Y coordinate of the upper coolant channel for the application of von Mises stress constraint at point G.

			dSe/de (1×10^{-1})
AVM and DDM			1.020
	% Perturb	dSe/de (1×10^{-1})	% Error
FDM (C)	0.2	1.020	4.76×10^{-3}
FDM (C)	2	1.016	0.37

Table 12
The design element sensitivities of von Mises stress with respect to X coordinate of the upper coolant channel for the application of von Mises stress constraint at point G.

			dSe/de (1×10^{-2})
AVM			−2.859
	% Perturb	dSe/de (1×10^{-2})	% Error
FDM (C)	0.2	−2.859	2.12×10^{-3}
FDM (C)	2	−2.858	0.03

sensitivities of von Mises stress with respect to Y and X coordinates of the upper coolant channel for the application of von Mises stress constraint at point G. It can be seen that the tendency to move the upper coolant channel in the Y-direction has a higher influence than in X-direction with respect to both von Mises stress constraints at points F and G. Also, the percentage errors were small thus proving the accuracy of the analytical method. In this example, only the DDM was used. This is because from the parameter sensitivity examples, it can be seen that clearly both methods yield the same results. In this section, the full picture of the shape sensitivity cannot be shown because of the calculated sensitivities were only evaluated on a certain number of elements in the die.

Thus, based on the cooling system design sensitivity, the degree to which the tendency to move the coolant channel either in X or Y-direction can be drawn with respect to the particular von Mises stress constraint in the die. Also, based on the above examples, from the practical point of view, it can be seen that generally if the coolant channel is moved in direction y, it will have a more significant impact on von Mises stress when compared with a move in direction x.

4. Conclusions

The Design Element Concept with the aim of reducing effort in sensitivity calculation in the optimisation process has been proposed. In this work, the die has been divided into five divisions of design elements, where the zones of defined design elements may correspondingly represent the number of blocks that make up the die. From the examples provided, it can be seen that as a number of divisions of design elements are increased, convergence of sensitivity is obtained for both displacement and von Mises stress constraints. Also, the shape sensitivities procedure of the coolant channels has been described, thus, enabling the coolant channels to be moved as an entity for each coolant channel for the shape optimisation problem. For the shape sensitivity, based on the calculated sensitivity, the extent to which the tendency to move the coolant channel either in X or Y-direction can be determined with respect to the particular von Mises stress constraint in the die.

References

[1] I.S. Cho, C.P. Hong, Modeling of microstructural evaluation in squeeze casting of an Al–4.5mass%Cu Alloy, ISIJ Int. 37 (1997) 1098–1106.
[2] A.J. Clegg, Precision Casting Processes, Pergamon Press, Berlin, 1991.
[3] S. Rajagopal, Squeeze casting: a review and update, J. Appl. Metalworking 1 (1981) 3–14.
[4] J.R. Franklin, A.A. Das, Squeeze Casting – a review of the status, Brit. Foundryman 77 (1984) 150–158.
[5] I.S. Cho, C.P. Hong, Evaluation of heat transfer coefficients at the casting/die interface in squeeze casting, Int. J. Cast Metals Res. 9 (1996) 227–232.
[6] O.C. Zienkiewicz, J.S. Campbell, Shape optimization and sequential linear Programming, in: R.H. Gallagher, O.C. Zienkiewicz (Eds.), Optimum Structural Design, Wiley, New York, 1973.
[7] D.A. Tortorelli, J.A. Tomasko, T.E. Morthland, J.A. Dantzig, Optimal design of nonlinear parabolic systems. Part II: Variable spatial domain with applications to casting optimization, Comput. Methods Appl. Mech. Eng. 113 (1994) 157–172.
[8] W. Sosnowski, I. Marczewska, A. Marczewski, Sensitivity based optimization of sheet metal forming tools, J. Mater. Process. Technol. 124 (2002) 319–328.
[9] C.H. Wu, Y.L. Su, Optimization of wedge-shaped parts for injection molding and injection compression molding, Int. Commun. Heat Mass Transfer 30 (2003) 215–224.
[10] A. Bikas, N. Pantelelis, A. Kanarachos, Computational tools for the optimal design of the injection moulding process, J. Mater. Process. Technol. 122 (2002) 112–126.
[11] J. Sienz, E. Hinton, Reliable structural optimization with error estimation, adaptivity and robust sensitivity analysis, Comput. Struct. 64 (1997) 31–63.
[12] B.K. Hwu, S.J. Lin, M.T. Jahn, Effects of process parameters on the properties of squeeze-cast SiCp-6061 Al metal–matrix composite, Mater. Sci. Eng. A 207 (1996) 135–141.
[13] S.W. Kim, D.Y. Kim, W.G. Kim, K.D. Woo, The study on characteristics of heat treatment of the direct squeeze cast 7075 wrought Al alloy, Mater. Sci. Eng. A 304–306 (2001) 721–726.
[14] A. Maleki, B. Niroumand, A. Shafyei, Effects of squeeze casting parameters on density, microstructure and hardness of LM13 alloy, Mater. Sci. Eng. A 428 (2006) 135–140.
[15] E.W. Postek, R.W. Lewis, D.T. Gethin, R.S. Ransing, Airgap prediction in the squeeze forming processes, Computer Methods in Mechanics, Gliwice, Poland, 2003.
[16] E.W. Postek, R.W. Lewis, D.T. Gethin, R.S. Ransing, Influence of initial stresses on the cast behaviour during squeeze forming processes, J. Mater. Process. Technol. 159 (2005) 338–346.
[17] R.W. Lewis, E.W. Postek, Z. Han, D.T. Gethin, A finite element model of the squeeze casting process, Int. J. Numer. Methods Heat Fluid Flow 16 (2006) 539–572.
[18] E.J. Haug, K.K. Choi, V. Komkov, Design Sensitivity Analysis of Structural Systems, Academic Press, London, 1986.
[19] T.D. Hien, M. Kleiber, Computational aspects in structural design sensitivity analysis for statics and dynamics, Comput. Struct. 33 (4) (1989) 939–950.
[20] H.J. Antunez, M. Kleiber, Sensitivity analysis of metal forming processes involving frictional contact in steady state, J. Mater. Process. Technol. 60 (1996) 485–491.
[21] H.J. Antunez, Thermo-mechanical modeling and sensitivity analysis for metal-forming operations, Comput. Methods Appl. Mech. Eng. 161 (1998) 113–125.
[22] S.H. Kim, H. Huh, Design sensitivity analysis of sheet metal forming processes with a direct differentiation method, J. Mater. Process Technol. 130–131 (2002) 504–510.
[23] D.E. Smith, D.A. Tortorelli, C.L. Tucker, Optimal design for polymer extrusion. Part I: Sensitivity analysis for nonlinear steady-state systems, Comput. Methods Appl. Mech. Eng. 167 (1998) 283–302.
[24] D.E. Smith, D.A. Tortorelli, C.L. Tucker, Optimal design for polymer extrusion. Part II: Sensitivity analysis for weakly-coupled nonlinear steady-state systems, Comput. Methods Appl. Mech. Eng. 167 (1998) 303–323.
[25] J.S. Arora, J.E.B. Cardoso, A design sensitivity analysis principle and its implementation into ADINA, Comput. Struct. 32 (3/4) (1989) 691–705.
[26] M.E. Botkin, Shape optimization of plate and shell structures, AIAA J. 20 (2) (1982) 268–273.
[27] R.W. Lewis, K. Morgan, H.R. Thomas, K.N. Seetharamu, The Finite Element Method in Heat Transfer Analysis, Wiley, Chichester, 1996.
[28] O.C. Zienkiewicz, The Finite Element Method, McGraw Hill, UK, 1977.
[29] R.W. Lewis, M.T. Manzari, D.T. Gethin, Thermal optimisation in the sand casting process, Eng. Comput. 18 (3/4) (2001) 392–416.
[30] E.J. Haug, K.K. Choi, V. Komkov, Design Sensitivity Analysis of Structural Systems, Academic Press, London, UK, 1986.
[31] M.A. Crisfield, Finite Elements and Solution Procedures for Structural Analysis, Linear Analysis, vol. 1, Pineridge Press, Swansea, UK, 1986.
[32] W.F. Chen, D.J. Han, Plasticity for Structural Engineers, Springer-Verlag, New York, 1988.
[33] <http://www.gknplc.com/>, 2003.
[34] J.T. Anderson, A Theoretical and Experimental Investigation into the Investment and Gravity Die Casting Processes. M.Phil Thesis, Swansea University, 1995.
[35] K. Ravindran, R.W. Lewis, Finite element modelling of solidification effects in mould filling, Finite Elem. Anal. Des. 31 (1998) 99–116.